Journal of Biomolecular NMR, 9 (1997) 181–200
ESCOM

J-Bio NMR 412

Triple-resonance NOESY-based experiments with improved spectral resolution: Applications to structural characterization of unfolded, partially folded and folded proteins

Ouwen Zhang[a,b], Julie D. Forman-Kay[b], David Shortle[c] and Lewis E. Kay[a]

[a]*Protein Engineering Network Centres of Excellence and Departments of Medical Genetics, Biochemistry and Chemistry, University of Toronto, Toronto, ON, Canada M5S 1A8*
[b]*Biochemistry Research Division, Hospital for Sick Children, 555 University Avenue, Toronto, ON, Canada M5G 1X8 and Department of Biochemistry, University of Toronto, Toronto, ON, Canada M5S 1A8*
[c]*Department of Biological Chemistry, Johns Hopkins University School of Medicine, Baltimore, MD 21205, U.S.A.*

Received 16 August 1996
Accepted 8 November 1996

Keywords: Heteronuclear, multidimensional NMR; NOE; Unfolded or partially folded proteins

Summary

NMR-based structural studies of macromolecules focus to a large extent on the establishment of interproton distances within the molecule based on the nuclear Overhauser effect (NOE). Despite the improvements in resolution resulting from multidimensional NMR experiments, the detailed characterization of disordered states of proteins or highly overlapped regions of folded molecules using current NMR methods remains challenging. A suite of triple-resonance NOESY-type pulse schemes is presented which require uniform ^{15}N and ^{13}C labeling and make use of the chemical shift dispersion of backbone ^{15}N and $^{13}C'$ (carbonyl) resonances to increase the spectral resolution. In particular, for the case of partially folded and unfolded proteins, the experiments exploit the fact that the dispersion of ^{15}N and $^{13}C'$ resonances is comparable to that observed in folded states. Ambiguities that arise in the assignment of NOEs as a result of the severe chemical shift degeneracy in ^{1}H and aliphatic ^{13}C nuclei are resolved, therefore, by recording the chemical shifts of ^{15}N or $^{13}C'$ either before or after the NOE mixing period. Applications of these methods to the study of the unfolded state of the N-terminal SH3 domain of drk (drkN SH3) and a partially folded large fragment of staphylococcal nuclease (SNase), Δ131Δ, are presented. In addition, an application to folded SNase in complex with the ligands thymidine 3',5'-bisphosphate (pdTp) and Ca^{2+} is illustrated which allows the assignment of NOEs between degenerate H^{α} protons or protons resonating close to water.

Introduction

Structural information about unfolded and partially folded proteins is of considerable interest in order to better understand the roles that these states play in directing protein folding pathways and in biomolecular recognition (Harrison and Aggarwal, 1990; Dobson, 1992; Shortle, 1993; Spolar and Record, 1994). NMR spectroscopy has become a useful method for characterizing these disordered states on a per residue basis (Wüthrich, 1994; Shortle, 1996). In the last few years, complete NMR assignments and limited structural analyses of several unfolded or partially folded proteins under various conditions have been reported (Neri et al., 1992; Arcus et al., 1994; Logan et al., 1994; Buck et al., 1995; Frank et al., 1995). These studies rely primarily on distance restraints based on nuclear Overhauser enhancement (NOE) experiments and use methods which were developed, and are in widespread use, for structural studies of native, folded proteins (Wüthrich, 1986; Clore and Gronenborn, 1991). However, the loss of ^{1}H and aliphatic ^{13}C chemical shift dispersion, due to conformational averaging, allows only limited, and often ambiguous, information to be obtained even for small unfolded proteins. The unambiguous assignment of NOEs is important for characterizing disordered states since they often demonstrate preferential sampling of

0925-2738/$ 6.00 + 1.00 © 1997 ESCOM Science Publishers B.V.

particular conformations. Although there is significant conformational heterogeneity in these systems, NOEs can be observed and used to characterize even a small population of preferentially structured conformers due to the steep distance dependence of the NOE. These small populations may be important for directing the folding pathway or for protein recognition in disordered states, including interactions with ligands or protein chaperonins (Harrison and Aggarwal, 1990; Dobson, 1992; Fersht, 1993; Shortle, 1993; Spolar and Record, 1994; Ellis and Hartl, 1996; Rassow and Pfanner, 1996).

Our interest in developing alternative approaches for the structural characterization of unfolded or partially folded states of proteins was stimulated by our studies of the unfolded state of the drkN SH3 domain (Zhang et al., 1994; Zhang and Forman-Kay, 1995). Src homology 3 (SH3) domains function to mediate protein interaction and localization and are found in cytoskeletal proteins and proteins involved in signal transduction (Mayer et al., 1988; Pawson, 1995). The drkN SH3 domain (59 residues) is the N-terminal SH3 domain of the *drosophila* signaling protein drk, a homologue of the mammalian Grb2 (Olivier et al., 1993; Simon et al., 1993). A dynamic equilibrium exists between the folded and unfolded states of the isolated SH3 domain under conditions close to physiological (Zhang and Forman-Kay, 1995). This protein provides, therefore, an excellent model for studying unfolded states under native solution conditions, similar to those in vivo. Sequential backbone resonance assignment and initial characterization of unfolded states of the protein have been reported previously (Zhang et al., 1994; Zhang and Forman-Kay, 1995), based primarily on ^{15}N-edited NOESY-HSQC (Zhang et al., 1994) data which suffer from a severe overlap of ^{1}H resonances. The ^{13}C and side-chain ^{1}H assignments of both folded and unfolded states have now been obtained using triple-resonance approaches (Bax and Grzesiek, 1993; Kay, 1995) and will be presented elsewhere.

A second model system for studies of disordered states of proteins under nondenaturing conditions is Δ131Δ, a partially folded 131-residue fragment of SNase with deletions of residues 4–12 and 141–149 of the wild-type protein (Alexandrescu et al., 1994a). Initial sequential assignment and structural characterization have been reported (Alexandrescu et al., 1994a). As in the case of the drkN SH3 domain, further structural characterization utilizing conventional methods for studying folded proteins was severely limited due to chemical shift degeneracy. Complete aliphatic side-chain ^{13}C resonance assignments of Δ131Δ have now been obtained (data not shown) using triple-resonance experiments in order to allow the new approaches we present here to be implemented.

Since the chemical shift dispersion of backbone ^{15}N and ^{13}C' resonances in unfolded or partially folded proteins is comparable to that in folded proteins, we have designed experiments which make more effective use of these nuclei to resolve NOE peaks that would otherwise overlap in conventional ^{15}N- or ^{13}C-edited NOESY spectra. We have focused on three classes of interproton distances: those between aliphatic protons, between aliphatic protons and backbone amide protons, and between amide protons exclusively. Applications of these methods to study the unfolded state of the drkN SH3 domain and Δ131Δ are presented. Spectra from simultaneous ^{13}C,^{15}N-edited NOESY (Pascal et al., 1993) and ^{15}N-edited NOESY-HSQC (Zhang et al., 1994) experiments are shown for comparison, in order to demonstrate the greater resolving power of these new experiments.

During the course of the development of these experiments, it became clear that a number of the pulse schemes would also be extremely useful in the study of folded proteins. Indeed, the problems associated with the assignment of NOEs in a folded protein which connect protons in highly overlapped spectral regions are identical to the difficulties encountered with NOE assignment in unfolded molecules. In the final section of the paper, we describe the application of an experiment that resolves aliphatic-H^{α} NOEs which we have found particularly useful for studying the folded state of SNase.

Materials and Methods

Uniformly labeled ^{15}N and ^{13}C drkN SH3 domain was overexpressed in *E. coli* BL21 cells grown at 37 °C in M9 minimal media with $^{15}NH_4Cl$ (1 g/l of culture) and $^{13}C_6$-glucose (3 g/l of culture) as the sole nitrogen and carbon sources. After harvesting, the cells were lysed by sonication in 50 mM Tris, 2 mM EDTA, 5 mM benzamidine, and 7 mM β-mercaptoethanol, pH 7.5. The protein was purified on a DE-52 ion-exchange column with a linear gradient of NaCl (0–0.75 M) followed by a Superdex-75 gel filtration column on an FPLC system (Pharmacia). Pure protein was concentrated and exchanged with 50 mM sodium phosphate, pH 6.0. The concentration of the protein was determined from amino acid analysis. The purity of the sample was estimated at over 98% from SDS-PAGE gel analysis. All spectra for this protein were acquired using a 1.5 mM sample dissolved in 90% H_2O, 10% D_2O, pH 6.0, 50 mM sodium phosphate at 5 °C.

The SNase Δ131Δ mutant was uniformly enriched with ^{15}N and ^{13}C and was expressed and purified according to previously published methods (Alexandrescu et al., 1994a). After extensive dialysis against distilled H_2O and lyophilization, 34.5 mg of Δ131Δ was dissolved in 90% H_2O, 10% D_2O with 1 mM sodium azide and the pH was adjusted to 5.3 with 1 N HCl, yielding a protein sample concentration of 4.5 mM. All experiments performed on this protein sample were recorded at 32 °C.

Fully folded SNase was a gift from Dr. Dennis Torchia (NIH) and was prepared as described previously (Torchia

et al., 1989). The sample conditions were: 1.5 mM SNase, 100 mM NaCl, 50 mM borate buffer, 5 mM pdTp, 10 mM Ca^{2+}, 35 °C.

Experiments were performed on either Varian UNITY Plus 500 MHz or UNITY Plus 600 MHz spectrometers equipped with pulsed field gradient units and actively shielded triple-resonance probe heads. The 2D ^{1}H-^{15}N-HSQC spectrum (Fig. 1a) was recorded with 128 and 512 complex points in t_1 and t_2, respectively, using the gradient sensitivity-enhanced approach (Kay et al., 1992; Schleucher et al., 1993) and a 2D H(N)CO spectrum (Kay et al., 1994) (Fig. 1b) was acquired with 128 and 512 complex points in the carbonyl and NH dimensions, respectively. The data set for the 3D simultaneous ^{13}C, ^{15}N-edited NOESY experiment (Pascal et al., 1993) comprised 128, 32 and 448 complex points in t_1, t_2 and t_3, respectively, and was recorded with spectral widths of 5499.8, 3000.0 and 8000.0 Hz (F1,F2,F3) at 500 MHz, respectively. The ^{15}N-edited NOESY-HSQC experiments (Zhang et al., 1994) utilized 128, 32 and 512 complex points in t_1, t_2 and t_3 and were acquired with spectral widths of 5499.8, 1063.5 and 8000.0 Hz (F1,F2,F3) at 500 MHz, respectively. The (H)C(CO)NH-TOCSY experiments (Montelione et al., 1992; Grzesiek et al., 1993; Logan et al., 1993) utilized 64, 26 and 512 complex points in t_1, t_2 and t_3 and were acquired with spectral widths of 7657.0, 1063.5 and 8000.0 Hz (F1,F2,F3) at 500 MHz, respectively. Table 1 shows experimental parameters for the spectra recorded using the novel pulse sequences described in the present paper. The parameters reported are the ones used for the Δ131Δ sample when spectra were recorded at 500 MHz. Similar parameters were utilized for the drkN SH3 domain. All NOESY experiments were recorded at a mixing time of 250 ms for the drkN SH3 domain. NOE-based experiments employed mixing times of 200, 150 or 75 ms for Δ131Δ. NOE-based experiments for the folded SNase were recorded with a mixing time of 75 ms.

All spectra were processed using NMRPipe software (Delaglio et al., 1995) and analyzed using the programs PIPP and CAPP (Garrett et al., 1991). In the acquisition dimensions for all experiments, a solvent suppression filter was applied to the data to minimize the residual water signal prior to apodization with a 65°-shifted squared sine-bell window function. The data were subsequently zero filled to 1024 complex points and Fourier transformed. Only the downfield half which includes the NH region was retained. For the t_1 dimension of experiments A, C, D, E and F (see Table 1), the data were apodized using a 65°-shifted sine-bell window function and zero filled to 128 complex points, followed by Fourier transformation, phasing, and elimination of the imaginary half of the signal. For the t_2 (^{15}N) dimension of these experiments, the size of the ^{15}N time domain was doubled via mirror image linear prediction (Zhu and Bax, 1990) (for A, since this is a constant time dimension) or forward–backward linear prediction (Zhu and Bax, 1992) (for C, D, E and F). The data were then apodized using a 72°-shifted squared sine-bell function, zero filled to 128 complex points, Fourier transformed, phased, and the imaginaries were eliminated. For experiment B, the t_2 (^{15}N) dimension was apodized using a 65°-shifted sine-bell window function and zero filled to 128 complex points, followed by Fourier transformation, phasing, and elimination of the imaginary half of the signal. The t_1 (^{15}N) dimension was doubled in size by mirror image linear prediction, apodized using a 72°-shifted squared sine-bell function, zero filled to 128 complex points, Fourier transformed, phased, and the imaginaries were eliminated. The final absorptive part of the 3D data set for each experiment included $128 \times 128 \times 512$ real points. Processing schemes for experiments modified by removing TOCSY transfer periods were the same as the corresponding experiments containing TOCSY periods.

Results and Discussion

Figure 1 illustrates 2D ^{1}H-^{15}N HSQC and 2D ^{1}H-$^{13}C'$ H(N)CO spectra of the drkN SH3 domain, 50 mM sodium phosphate, pH 6.0. Under these conditions, the

TABLE 1
EXPERIMENTAL PARAMETERS FOR DATA SETS RECORDED AT 500 MHz

Experiment	SW (Hz)			np			t_1 (ms)	t_2 (ms)	t_3 (ms)	ns	Time (h)
	F1	F2	F3	t_1	t_2	t_3					
A	7657.0 (^{13}C)	1063.5	8000.0	64	26	512	8.36	24.4	64.0	32	86
B	1063.5 (^{15}N)	1063.5	8000.0	28	28	512	26.3	26.3	64.0	48	92
C	1063.5 (^{15}N)	1063.5	8000.0	28	64	512	26.3	60.2	64.0	32	68
D	1250.0 ($^{13}C'$)	1063.5	8000.0	30	48	512	24.0	45.1	64.0	32	70
E	1000.0 ($^{13}C'$)	1063.5	8000.0	36	32	512	36.0	30.1	64.0	32	62
F	1063.5 (^{15}N)	1063.5	8000.0	64	32	512	60.2	30.1	64.0	16	50

A: C_i-NOESY-TOCSY-$N_{j+1}H_{j+1}$; B: N_{i+1}-NOESY-$N_{j+1}H_{j+1}$; C: N_{i+1}-TOCSY-NOESY-N_jH_j; D: (HN)CO_i-TOCSY-NOESY-N_jH_j; E: (HCA)CO_i-NOESY-N_jH_j; F: HSQC-NOESY-HSQC; SW (F1), SW (F2), SW (F3): spectral widths in the F1, F2(^{15}N) and F3(NH) dimensions; np(t_1), np(t_2), np(t_3): complex number of points in the F1, F2 and F3 dimensions; t_1, t_2, t_3: acquisition times in each of the three dimensions; ns: number of scans per FID; Time: total acquisition time of each experiment.

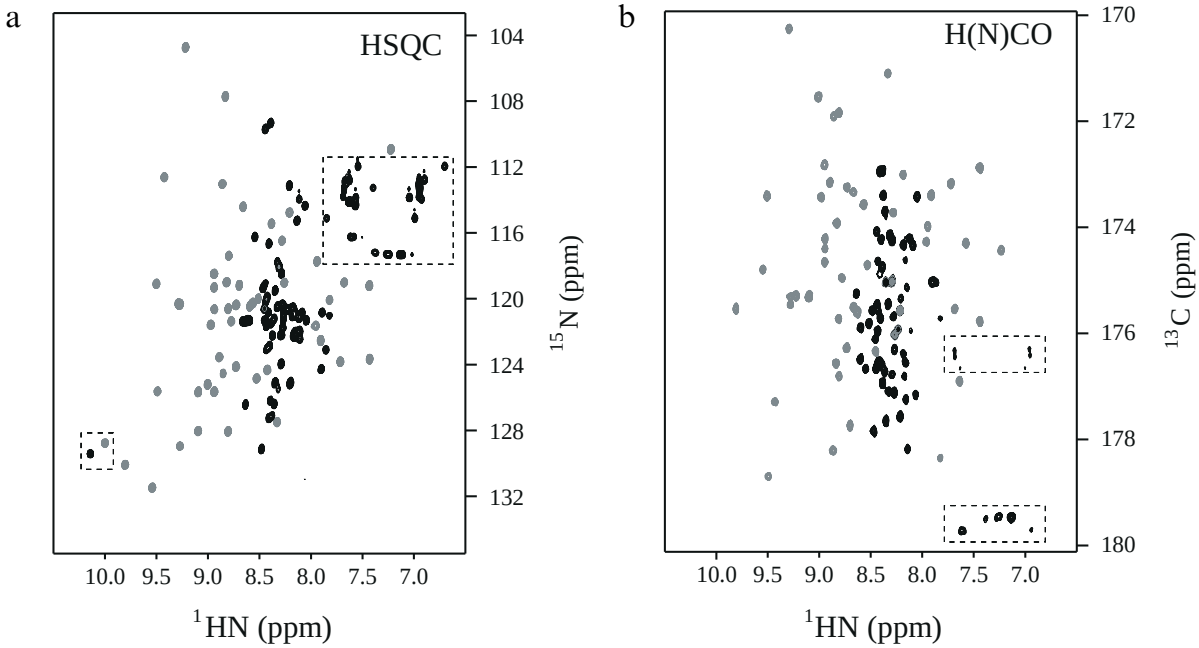

Fig. 1. ^{1}H-^{15}N HSQC (a) and ^{1}H-^{13}C' H(N)CO (b) spectra of the drkN SH3 domain at 5 °C, pH 6.0, 50 mM sodium phosphate recorded at a ^{1}H frequency of 600 MHz. Gray peaks are from the folded state and black peaks are from the unfolded state. Peaks in dashed-line boxes are from side-chain ^{15}N and ^{13}C' resonances, with no distinction between peaks of the folded and unfolded states except for the Trp^{36} indole peaks in (a).

protein undergoes slow exchange between folded and unfolded states, with a ratio of folded to unfolded conformers of approximately 1:1 (Zhang and Forman-Kay, 1995). Therefore, two sets of peaks are present, one for each state. The backbone NH chemical shifts of the folded state (gray peaks) span 7.2–9.8 ppm (2.6 ppm), while the NH chemical shifts of the unfolded state (black peaks) span only 7.8–8.6 ppm (0.8 ppm). In contrast, the dispersion of ^{15}N and ^{13}C' shifts in the unfolded state is not as dramatically reduced relative to the folded state, from 27 ppm (folded) to 20 ppm (unfolded) and from 8.8 ppm (folded) to 5.5 ppm (unfolded), respectively. Unlike resonances in the folded state of the drkN SH3 domain, where aliphatic ^{1}H or ^{13}C chemical shifts differ significantly from their random coil values ($|\Delta\delta\ ^{1}H|$ up to 1.4 ppm and $|\Delta\delta\ ^{13}C|$ up to 6.7 ppm), only very small deviations from random coil values ($|\Delta\delta\ ^{1}H| < 0.2$ ppm and $|\Delta\delta\ ^{13}C| <$ 1 ppm) are found for aliphatic resonances in the unfolded state. The chemical shifts of specific aliphatic ^{1}H and ^{13}C nuclei of the same residue type are often almost identical. Comparisons of the chemical shift dispersion of NH, ^{15}N, ^{13}C' and aliphatic ^{1}H and ^{13}C nuclei of Δ131Δ with the dispersion of the corresponding nuclei of wild-type staphylococcal nuclease demonstrate similar results.

As described above, our strategy to overcome this severe resonance overlap problem for ^{1}H and aliphatic ^{13}C resonances in NOE-based experiments is to transfer magnetization before and/or after an NOE mixing period to relatively well-resolved nuclei. Both ^{15}N and ^{13}C' chemical shifts can be recorded in order to resolve NOE peaks between protons attached to nuclei with resonance overlap. However, we focus primarily on pulse schemes using ^{15}N as the resolving nucleus since in this case it is straightforward to utilize gradient sensitivity-enhanced methods (Kay et al., 1992; Schleucher et al., 1993; Muhandiram and Kay, 1994). When the degeneracy of ^{15}N chemical shifts leads to difficulty in NOE assignment, ^{13}C' chemical shifts can then be used to obtain complementary information to make the assignment unambiguous. Because of the necessity of recording backbone ^{15}N and ^{13}C' chemical shifts, the pulse sequences tend to be more complex than previously described NOE-based pulse schemes. The methods will, therefore, be of highest sensitivity for regions of the molecule that enjoy moderately long transverse relaxation times. In this regard it is of interest that, for 12 residues examined in the drkN SH3 domain at 14 °C, the average ^{15}N T_2 value measured in the unfolded state is 220 ms while in the folded state it is 150 ms (Farrow et al., 1995). It is worthwhile to note that a similar approach for resolving NOEs has been successful in the structural analyses of complex carbohydrates by NMR, where NOE signals involving degenerate protons are transferred via isotropic mixing to neighboring, well-resolved protons (Van Halbeek, 1994).

The pulse schemes presented here are derived from conventional ^{15}N,^{13}C triple-resonance experiments. The ^{15}N-HSQC-NOESY-HSQC experiment (Frenkiel et al., 1990; Ikura et al., 1990) is included for completeness, although it has been described previously and does not utilize triple-resonance methodology. A large number of triple-resonance pulse sequences have been discussed in detail in the literature previously (Bax, 1994). With this

in mind, we will not provide a detailed explanation of each experiment here but will rather highlight the unique features of these pulse sequences and provide a rationale for their design as well as a discussion and analysis of the spectra. Pulsed field gradients are employed in all of the experiments in order to minimize both the artifact content (Bax and Pochapsky, 1992) and the residual water in spectra as well as to select for the coherence transfer pathway whereby magnetization passes through nitrogen

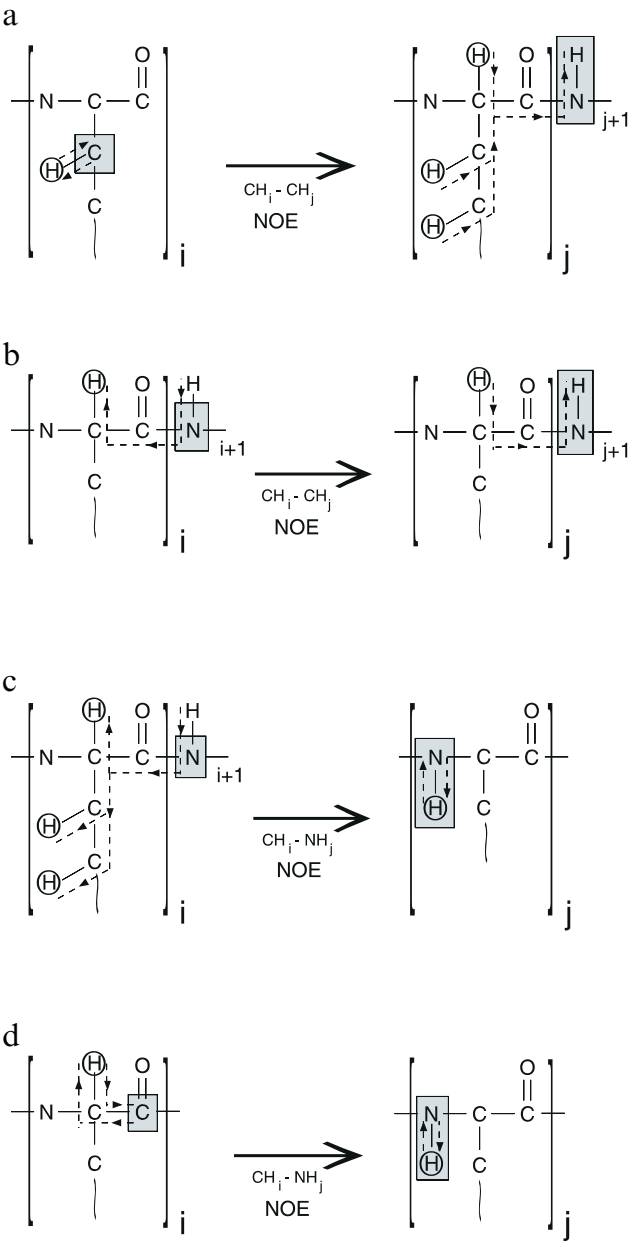

Fig. 2. Schematic diagrams showing the magnetization transfer pathways for the NOE-based experiments described in the text. Protons in residues i and j that are involved in the NOE transfer are circled. Nuclei whose chemical shifts are recorded are shown in shaded rectangles. (a) 3D C_i-NOESY-TOCSY-$N_{j+1}H_{j+1}$ experiment; (b) 3D N_{i+1}-NOESY-$N_{j+1}H_{j+1}$ experiment; (c) 3D N_{i+1}-TOCSY-NOESY-N_jH_j experiment; (d) 3D (HCA)CO_i-NOESY-N_jH_j experiment.

in the final portion of each of the sequences (Kay et al., 1992; Muhandiram and Kay, 1994). An enhanced sensitivity approach is used to optimize the signal-to-noise ratio (S/N), especially critical for these long sequences incorporating multiple magnetization transfer steps and aimed at detecting weak conformational preferences in a primarily disordered ensemble. In addition, saturation/dephasing of water magnetization is kept to a minimum by ensuring that (i) homospoil gradient pulses are applied only when the water magnetization is stored along the z-axis; and (ii) the water magnetization is placed along the +z-axis immediately prior to detection (Grzesiek and Bax, 1993; Kay et al., 1994; Stonehouse et al., 1994). This is also particularly important for disordered states in which amide proton exchange with solvent is much greater, on average, than for stable, folded proteins.

The experiments described below provide three different types of NOE connectivities. The C_i-NOESY-TOCSY-$N_{j+1}H_{j+1}$, N_{i+1}-NOESY-$N_{j+1}H_{j+1}$ and (HN)CO_i-NOESY-$N_{j+1}H_{j+1}$ experiments provide NOEs between two aliphatic protons. The N_{i+1}-TOCSY-NOESY-N_jH_j, (HN)CO_i-TOCSY-NOESY-N_jH_j and (HCA)CO_i-TOCSY-NOESY-N_jH_j experiments provide NOEs between aliphatic and NH protons. NOEs between two amide protons are observed in the ^{15}N-HSQC-NOESY-HSQC experiment. The nomenclature used for the triple resonance experiments gives the identity of the nuclei whose chemical shifts are recorded for assigning an NOE between two protons in residues i (origination) and j (destination). The term TOCSY refers to a carbon isotropic mixing sequence which transfers magnetization between aliphatic carbon resonances of a residue, either starting or landing on the C^{α} spin. In general, INEPT (Morris and Freeman, 1979) transfer periods are not indicated in the nomenclature, with the exception of experiments which record carbonyl chemical shift, in which case we distinguish between HNCO- and HCACO-type transfers (Kay et al., 1990). For example, the (HN)CO_i-TOCSY-NOESY-N_jH_j and (HCA)CO_i-TOCSY-NOESY-N_jH_j experiments differ only in beginning magnetization transfer pathways and not in the chemical shifts recorded or NOEs detected. As in previous triple-resonance literature (Kay et al., 1990), parentheses denote spins whose chemical shifts are not recorded, but through which magnetization is transferred. For many of these experiments, the sequences can be modified by removing the carbon TOCSY period(s) before and/or after the NOE mixing time. Thus, in the C_i-NOESY-$N_{j+1}H_{j+1}$ experiment, NOEs between aliphatic protons and α protons are observed, while NOEs between α protons and NH protons are observed in the (HN)CO_i-NOESY-N_jH_j and (HCA)CO_i-NOESY-N_jH_j experiments. Figure 2 summarizes the recorded nuclei and the flow of magnetization that is involved in some of these experiments.

As described in the Introduction section, a number of

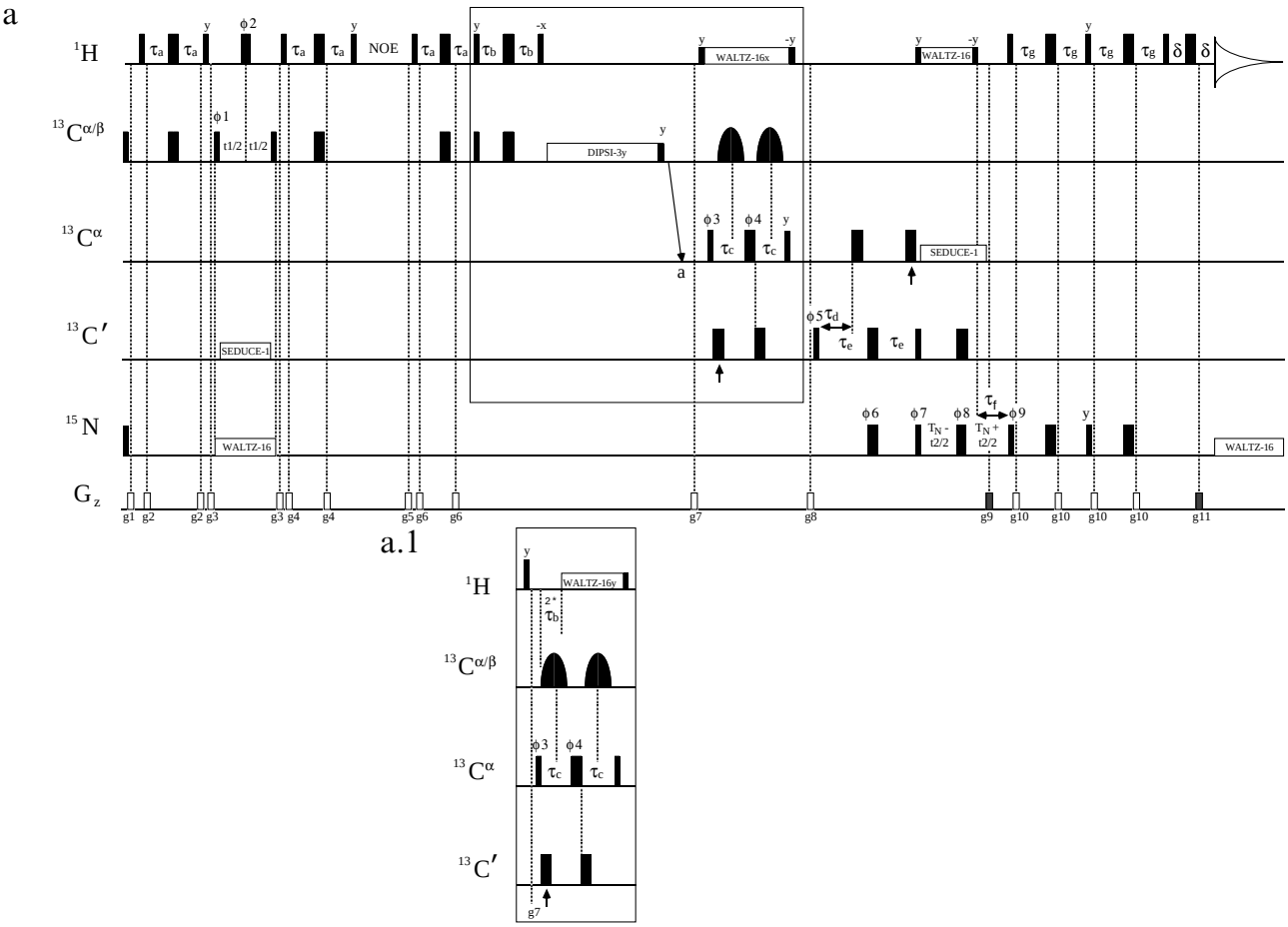

Fig. 3. Pulse schemes for the structural characterization of unfolded or partially folded proteins. All narrow (wide) pulses are applied with a flip angle of 90° (180°). Unless indicated otherwise, pulses are applied along the x-axis. If not indicated otherwise, ^{1}H WALTZ-16 (Shaka et al., 1983) is applied with pulses along the ±x-axes; W_y denotes WALTZ decoupling applied along the y-axis. The ^{1}H and ^{15}N carriers are centered at the water frequency, 4.9 ppm (at 5 °C) or 4.7 ppm (at 32 °C), and 119 ppm, respectively. Proton pulses are applied using a 30 kHz field, with the exception of the selective water 90° pulses (indicated by the shaped ^{1}H pulses in the sequences) which are applied as 2 ms rectangular pulses or as 2 ms pulses having the SEDUCE-1 (McCoy and Mueller, 1992) profile and the ^{1}H 90° pulses immediately flanking the WALTZ-16 (Shaka et al., 1983) decoupling intervals which are applied using a 6.1 kHz field. ^{1}H WALTZ (Shaka et al., 1983) decoupling is achieved using a 6.0 kHz field. High-power ^{15}N pulses are applied using a 6.1 kHz field and a 1 kHz decoupling field during acquisition is employed. All carbon pulses are applied using a single frequency source and, unless otherwise indicated, are rectangular in shape. All gradients are rectangular and are applied along the z-direction. Decoupling is interrupted during the application of the gradient pulses (Kay, 1993). In the case of ^{1}H decoupling, the water magnetization must first be 'returned' to the z-axis prior to application of the gradient pulse and subsequently rotated to the decoupling axis prior to the continuation of decoupling (Kay et al., 1994). Note that all pulse widths reported for carbon were those used at 500 MHz (^{1}H frequency).

Sequences (a) and (a.1), C_i-NOESY-TOCSY-$N_{j+1}H_{j+1}$ (a) and C_i-NOESY-$N_{j+1}H_{j+1}$ (a.1): The carrier for $^{13}C^{\alpha/\beta}$ pulses is positioned at 43 ppm and for $^{13}C^{\alpha}$ pulses at 58 ppm. The carbon carrier is jumped from 43 to 58 ppm at point a. The first six $^{13}C^{\alpha/\beta}$ pulses are rectangular and are applied with a field strength of 21 kHz. The $^{13}C^{\alpha/\beta}$ 180° pulse immediately before DIPSI-3 (Shaka et al., 1988) (applied with pulses of phase ±y at 8 kHz) employs a 9.6 kHz field to minimize the excitation of C' spins. Because of phase changes associated with large changes in the power levels of carbon pulses, the $^{13}C^{\alpha/\beta}$ 90° pulse prior to the DIPSI-3 mixing scheme is applied with a field strength of 12 kHz. The $^{13}C^{\alpha}$ 90° and 180° pulses are applied using field strengths of 3.8 and 8.6 kHz, respectively, so that the application of $^{13}C^{\alpha}$ pulses minimizes the excitation of $^{13}C'$ spins (Kay et al., 1990). The $^{13}C'$ 90° and 180° pulses are applied as 118 ppm phase-modulated pulses using a field strength of 3.8 kHz (Boyd and Soffe, 1989; Patt, 1992). The positions of the Bloch–Siegert compensation pulses (Vuister and Bax, 1992) are indicated by vertical arrows under the pulses. $^{13}C'$ decoupling is achieved using a 133 ppm cosine-modulated WALTZ-16 (Shaka et al., 1983) field employing pulses having the SEDUCE-1 (McCoy and Mueller, 1992) profile (330 μs 90° pulses). $^{13}C^{\alpha}$ decoupling is achieved using pulses with the SEDUCE-1 (McCoy and Mueller, 1992) profile with a width of 330 μs (on resonance). ^{13}C isotropic mixing is accomplished using two cycles of the DIPSI-3 scheme (Shaka et al., 1988). If $^{13}C^{\beta}$ decoupling is not utilized, the value of τ_c is set to 2.7 ms to minimize signal loss due to the passive $^{13}C^{\alpha}$-$^{13}C^{\beta}$ coupling. $^{13}C^{\beta}$ decoupling can be achieved using 3.6 ms cosine-modulated G3 pulses to selectively invert C^{β} magnetization while not affecting the $^{13}C^{\alpha}$ region (Emsley and Bodenhausen, 1987; McCoy, 1995). The value of τ_c is 3.9 ms in this case and a single cosine-modulated G3 pulse is employed for each τ_c period. Alternatively, $^{13}C^{\beta}$ decoupling can be achieved by employing schemes which make use of CHIRP pulses (Böhlen et al., 1989). In this case τ_c is set to 3.6 ms. In order to construct each of the CHIRP pulses, the following procedure is employed. A 1.8 ms CHIRP pulse swept from 23 to 47 ppm is constructed. The B_1 field is ramped from zero to maximum intensity (740 Hz) using a sine ramping function over the first 30% of the pulse. In a similar manner the intensity is ramped down over the final 30% of the pulse. Two such pulses, one with phase x and the other –x, are concatenated. A 3.6 ms pulse (phase x) extending from 14 to 26 ppm is generated (for the C^{β} decoupling of alanine residues) in the same manner and added to the (x,–x) pulse train. The intensity ratio of the 3.6 ms (C^{β}) and the (x,–x) pulses is 1:2 (note that since the frequency sweep of the C^{β}

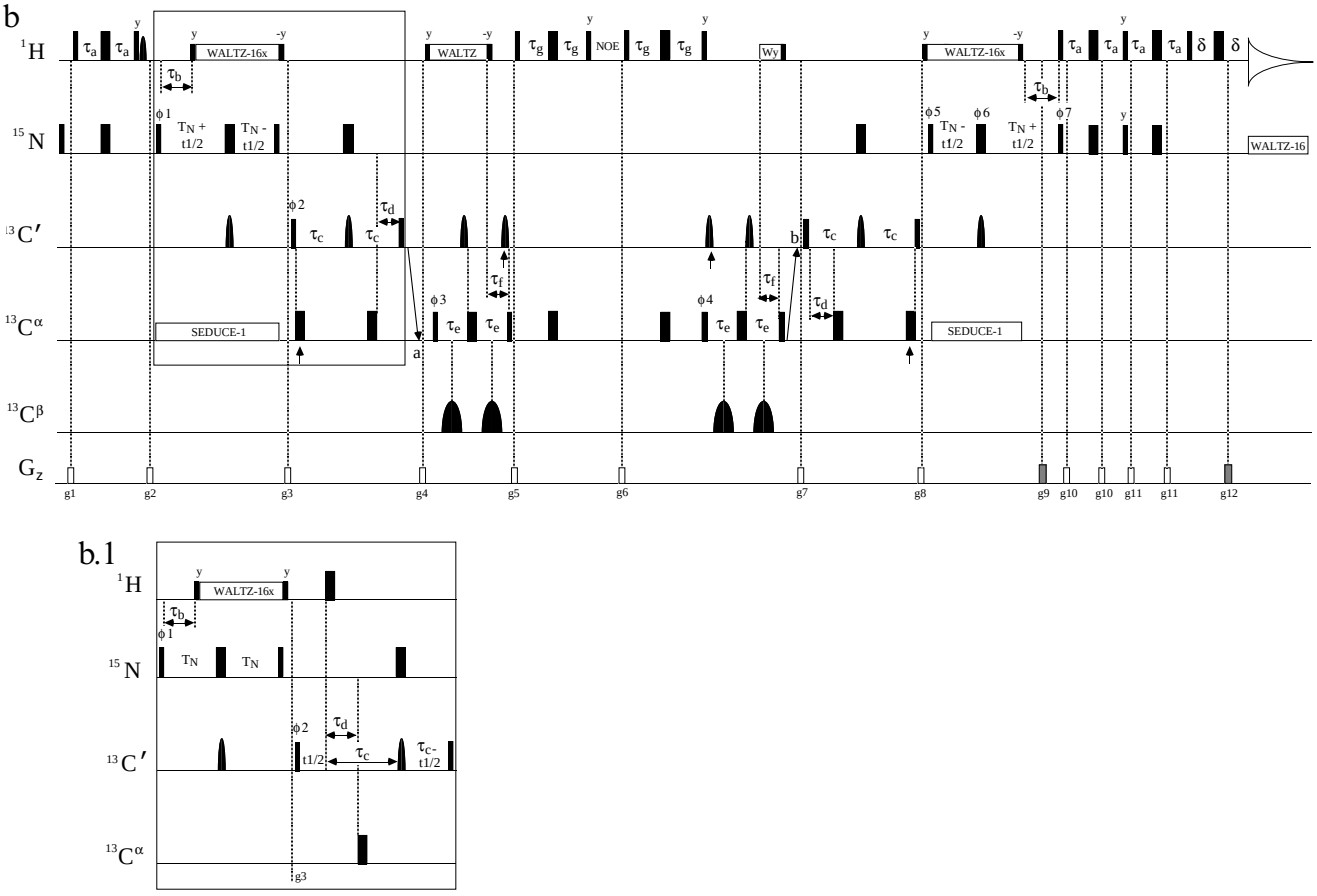

pulse is half that of the other CHIRP pulses and the sweep time double, the rf field must be 50% that used for the (x,–x) pulses) (Kupce and Freeman, 1995; Kupce and Wagner, 1995). This entire decoupling element is applied once for each τ_c period. Note that the phases of all the constituent CHIRP pulses are inverted for the second τ_c period. For C_i-NOESY-$N_{j+1}H_{j+1}$, the rectangle in (a) is replaced by (a.1). The delay between the first $^{13}C^{\alpha}$ 90° (phase $\phi3$) and the start of WALTZ-16y decoupling in (a.1) is $2\tau_b = 2.1$ ms. The following parameters are employed in both pulse schemes: $\tau_a = 1.8$ ms, $\tau_b = 1.05$ ms (this delay can be increased to 1.7 ms to optimize the sensitivity for AX spin systems at the expense of eliminating signals from CH_2 and CH_3 groups), $\tau_d = 4.4$ ms, $\tau_e = 12.4$ ms, $\tau_f = 5.5$ ms, $T_N = 12.4$ ms, $\tau_g = 2.3$ ms, $\delta = 0.75$ ms. The phase cycling employed is $\phi1 = 2(x),2(-x)$; $\phi2 = (x,-x)$; $\phi3 = 8(x),8(-x)$; $\phi4 = 4(x),4(-x)$; $\phi5 = 4(x),4(-x)$; $\phi6 = 8(x),8(-x)$; $\phi7 = x$; $\phi8 = (x,-x)$; $\phi9 = x$; rec. $= 2(x),4(-x),2(x),2(-x),4(x),2(-x)$. Quadrature in F1 is obtained via States-TPPI (Marion et al., 1989) of $\phi1$. For each value of t_2, N- and P-type coherences are obtained by recording data sets where the sign of the gradient g9 is inverted and 180° is added to the phase $\phi9$ for the second data set. Data sets, obtained in an interleaved manner for positive and negative g9 values, are stored in separate memory locations and pure absorptive line shapes in the ^{15}N dimension are generated by adding and subtracting the N- and P-type data sets, storing the new data sets separately and applying a 90° zero-order phase correction in the acquisition dimension to one (not both) of the new data sets (Kay et al., 1992). The phase $\phi7$ and the phase of the receiver are incremented by 180° for each increment of t_2 (Marion et al., 1989). The durations and strengths of the gradients are g1 = (1.0 ms, 6 G/cm), g2 = (0.1 ms, 8 G/cm), g3 = (0.5 ms, 6 G/cm), g4 = (0.1 ms, 10 G/cm), g5 = (0.5 ms, 12 G/cm), g6 = (0.2 ms, 4 G/cm), g7 = (0.5 ms, 5 G/cm), g8 = (0.5 ms, 8 G/cm), g9 = (1.25 ms, 30 G/cm), g10 = (0.5 ms, 5 G/cm), g11 = (0.125 ms, 29 G/cm).

Sequences (b) and (b.1), N_{i+1}-NOESY-$N_{j+1}H_{j+1}$ (b) and (HN)CO_i-NOESY-$N_{j+1}H_{j+1}$ (b.1): For (HN)CO_i-NOESY-$N_{j+1}H_{j+1}$, the rectangle in (b) is replaced by (b.1). Carbonyl 180° pulses (shaped pulses in the figure, length 230 μs) are applied using the SEDUCE-1 (McCoy and Mueller, 1992) profile. All carbon pulses are generated with the carrier centered at 176 ppm until point a in the sequence when the carbon carrier is jumped from 176 to 58 ppm. At point b the carbon carrier is returned to 176 ppm. The $^{13}C'$ 180° pulses between points a and b are applied as 118 ppm phase-modulated pulses (Boyd and Soffe, 1989; Patt, 1992). All $^{13}C'$ and $^{13}C^{\alpha}$ 90° pulses are applied using a field strength of 3.8 kHz so that the application of $^{13}C'$ pulses minimizes the excitation of $^{13}C^{\alpha}$ spins and vice versa (Kay et al., 1990). The $^{13}C^{\alpha}$ 180° pulses are applied at a field strength of 8.6 kHz (the two pulses before a and after b are 118 ppm phase-modulated pulses). The positions of the Bloch–Siegert compensation pulses (Vuister and Bax, 1992) are indicated by arrows under the appropriate pulses. $^{13}C^{\alpha}$ decoupling is achieved using a 118 ppm cosine-modulated WALTZ-16 (Shaka et al., 1983) field employing pulses having the SEDUCE-1 (McCoy and Mueller, 1992) profile (310 μs 90° pulses). $^{13}C^{\beta}$ decoupling can be applied as described for sequence (a). The delays are as follows: $\tau_a = 2.5$ ms, $\tau_b = 5.5$ ms, $\tau_c = 12.0$ ms, $\tau_d = 4.3$ ms, $\tau_f = 2.1$ ms, $\tau_g = 1.7$ ms, $T_N = 13.5$ ms, $\delta = 0.75$ ms. In the absence of $^{13}C^{\beta}$ decoupling τ_c is set to 2.7 ms. If G3 inversion pulses or CHIRP decoupling is employed τ_c is set to 3.9 or 3.6 ms, respectively. The phase cycling employed is $\phi1 = (x,-x)$; $\phi2 = 2(x),2(-x)$; $\phi3 = 4(x),4(-x)$; $\phi4 = 8(x),8(-x)$; $\phi5 = x$; $\phi6 = 8(x),8(-x)$; $\phi7 = x$; rec. $= (x,2(-x),x,-x,2(x),2(-x),2(x),-x,x,2(-x),x)$. Quadrature in F1 is achieved via States-TPPI (Marion et al., 1989) of $\phi1$ for (b) or $\phi2$ for (b.1). For each value of t_2, N- and P-type coherences are obtained by recording data sets where the sign of the gradient g9 is inverted and 180° is added to the phase $\phi7$. The phase $\phi5$ and the phase of the receiver are incremented by 180° for each increment of t_2. The durations and strengths of the gradients are g1 = (0.5 ms, 8 G/cm), g2 = (1.0 ms, 10 G/cm), g3 = (1.0 ms, 6 G/cm), g4 = (0.2 ms, 5 G/cm), g5 = (0.5 ms, 8 G/cm), g6 = (1.0 ms, 15 G/cm), g7 = (0.4 ms, 5 G/cm), g8 = (0.3 ms, −5 G/cm), g9 = (1.25 ms, 30 G/cm), g10 = (0.3 ms, 1.25 G/cm), g11 = (0.5 ms, 2 G/cm), g12 = (0.125 ms, 29 G/cm).

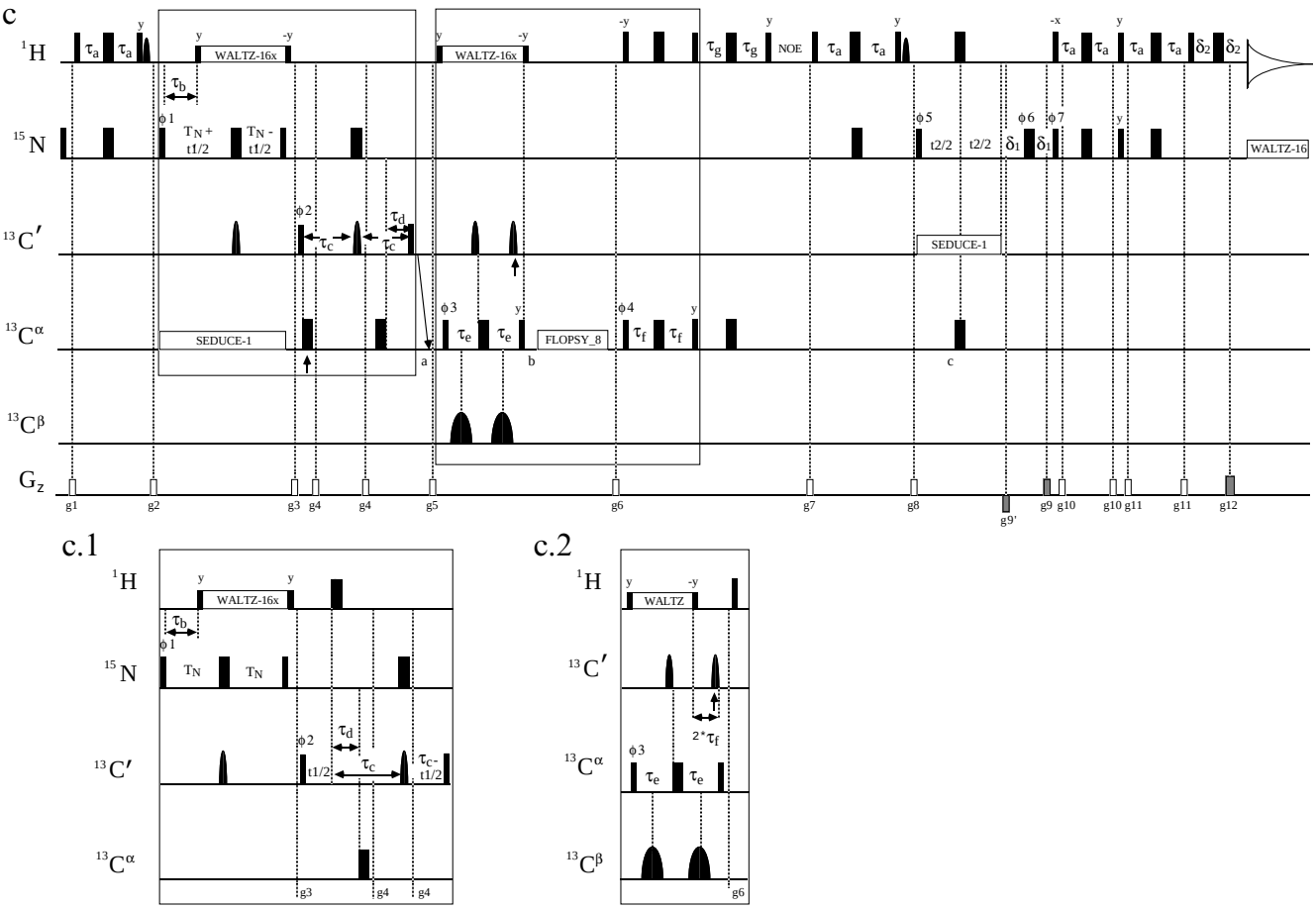

Fig. 3. *Sequences (c), (c.1) and (c.2)*: The pulse scheme in (c) corresponds to N_{i+1}-TOCSY-NOESY-N_jH_j. For (HN)CO_i-TOCSY-NOESY-N_jH_j the first rectangle in (c) is replaced by (c.1), while in the N_{i+1}-NOESY-N_jH_j sequence the second rectangle in (c) is replaced by (c.2). For (HN)CO_i-NOESY-N_jH_j, the two rectangles in (c) should be replaced by (c.1) and (c.2). Durations of pulses and pulse shapes are as described in (b) with a number of exceptions listed below. At point a in the sequence the carbon carrier is jumped from 176 to 58 ppm, at point b the carrier is placed at 43 ppm, and the carrier is moved to 58 ppm immediately after gradient g8. Therefore the carbon pulse at point c is applied 'on resonance' while C' decoupling is achieved using a 118 ppm cosine-modulated field. ^{13}C isotropic mixing is accomplished using seven cycles of an 8 kHz FLOPSY-8 mixing scheme (Kadkhodaie et al., 1991). All $^{13}C^{\alpha}$ pulses after the FLOPSY-8 scheme are applied at a field strength of 21 kHz. The positions of the Bloch–Siegert compensation pulses (Vuister and Bax, 1992) are indicated by arrows under the appropriate pulses. The delays employed are as follows: $\tau_a = 2.5$ ms, $\tau_b = 5.5$ ms, $\tau_c = 12.0$ ms, $\tau_d = 4.3$ ms, $\tau_f = 1.1$ ms, $\tau_g = 1.7$ ms, $T_N = 13.5$ ms, $\delta_1 = 1.5$ ms, $\delta_2 = 0.75$ ms. The duration of the delay τ_e is as described in (a) and (b). The phase cycling employed is $\phi1 = (x,-x)$; $\phi2 = 2(x),2(-x)$; $\phi3 = 4(x),4(-x)$; $\phi4 = 8(x),8(-x)$; $\phi5 = x$; $\phi6 = 8(x),8(-x)$; $\phi7 = x$; rec. = x,2(–x),x,–x,2(x),–x. For the subsequent eight scans the phase of the receiver is inverted. Quadrature in F1 is achieved via States-TPPI (Marion et al., 1989) of $\phi1$ for (c) or $\phi2$ for (c.1). For each value of t_2, N- and P-type coherences are obtained by recording data sets where the signs of the gradients g9 and g9' are inverted and 180° is added to the phase $\phi7$. The phase of $\phi5$ and the phase of the receiver are incremented by 180° for each increment of t_2. The durations and strengths of the gradients are g1 = (0.5 ms, 8 G/cm), g2 = (1.0 ms, 10 G/cm), g3 = (1.0 ms, 6 G/cm), g4 = (0.2 ms, 15 G/cm), g5 = (0.2 ms, 5 G/cm), g6 = (0.5 ms, 8 G/cm), g7 = (1.0 ms, 15 G/cm), g8 = (1.0 ms, –10 G/cm), g9 = (1.25 ms, 15 G/cm), g9' = (1.25 ms, –15 G/cm), g10 = (0.3 ms, 1.25 G/cm), g11 = (0.5 ms, 2 G/cm), g12 = (0.125 ms, 29 G/cm).

the methods that have been derived are well suited for the study of folded protein states as well. For these applications the TOCSY transfer periods are not utilized in the experiments. For clarity, we shall focus on applications to unfolded and partially folded protein states exclusively until the final section when an application to folded SNase is presented.

Aliphatic-aliphatic NOEs

In general, side chains of an unfolded protein do not pack as tightly as in a folded protein. However, conformational preferences within the unfolded state, such as those which may function to initiate protein folding, could involve side-chain–side-chain interactions. Specific contacts between hydrophobic side chains in the urea-denatured form of 434-repressor have been demonstrated (Neri et al., 1992). Although these interactions are important for the full characterization of structure in disordered states, aliphatic ^1H-^1H NOEs have not been analyzed in a systematic manner in previously reported structural studies of unfolded or partially folded proteins (Alexandrescu et al., 1994a,b; Logan et al., 1994; Arcus et al., 1995; Buck et al., 1995; Frank et al., 1995; Zhang and Forman-Kay, 1995). This is due to the extremely

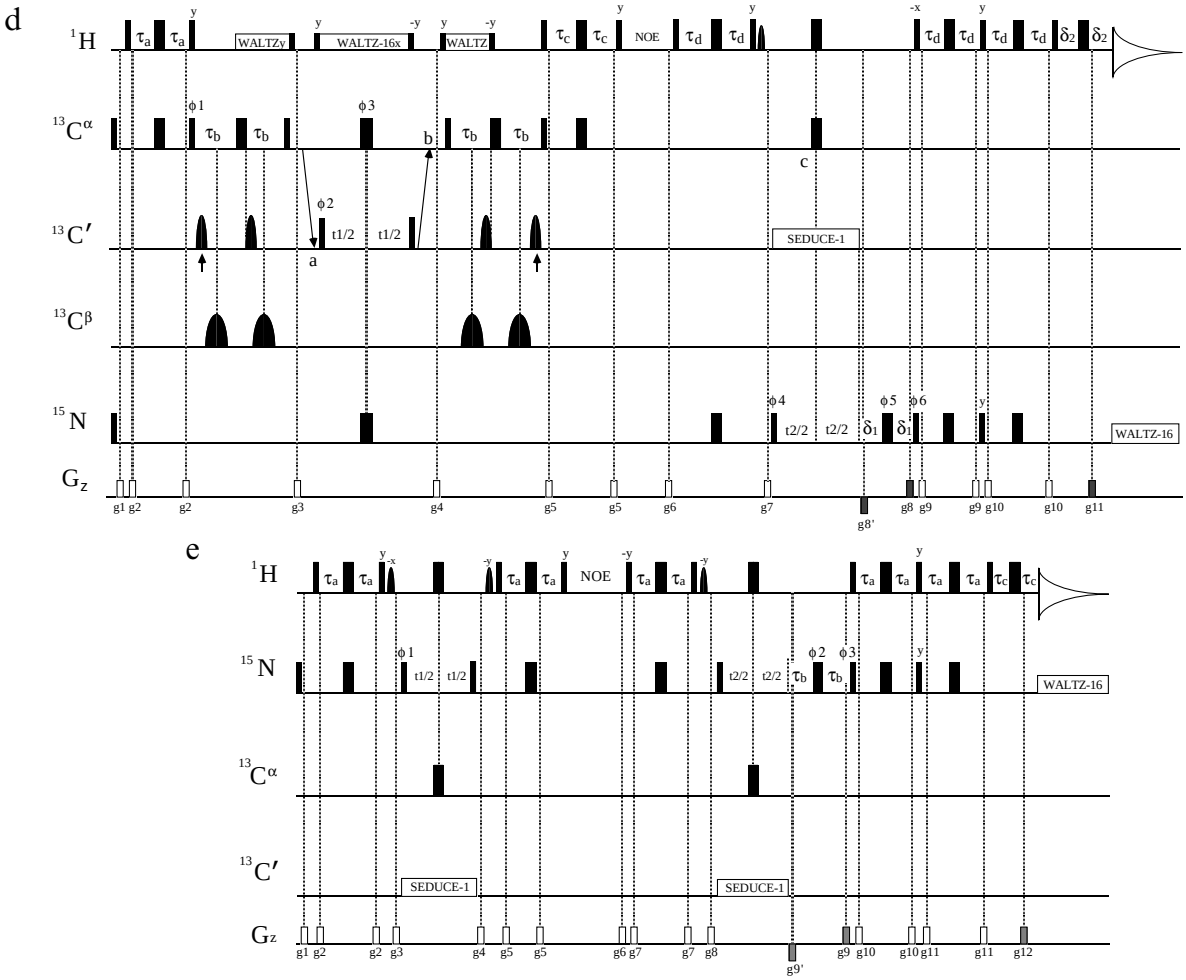

Fig. 3. *Sequence (d)*, (HCA)CO$_i$-NOESY-N$_j$H$_j$: The carrier for carbon pulses is initially positioned at 58 ppm and jumped to 176 ppm at point a, and then to 58 ppm at point b. All carbonyl 180° pulses are applied with a SEDUCE-1 (McCoy and Mueller, 1992) profile and a width of 230 μs. The ^{13}C' and ^{13}C$^\alpha$ 90° pulses are applied using a field strength of 3.8 kHz so that the application of ^{13}C' pulses minimizes the excitation of ^{13}C$^\alpha$ spins and vice versa as described above, and the ^{13}C$^\alpha$ 180° pulses are applied with a field of 8.6 kHz. The ^{13}C$^\alpha$ pulse at point c is applied using a field strength of 21 kHz. The positions of the Bloch–Siegert compensation pulses (Vuister and Bax, 1992) are indicated by vertical arrows. ^{13}C' decoupling is achieved using a 118 ppm cosine-modulated WALTZ-16 (Shaka et al., 1983) field employing pulses having the SEDUCE-1 (McCoy and Mueller, 1992) profile (330 μs 90° pulses). ^{13}C$^\beta$ decoupling is as described above. The delays employed are as follows: $\tau_a = 1.7$ ms, $\tau_b = 3.6$ ms, $\tau_c = 1.7$ ms, $\tau_d = 2.5$ ms, $\delta_1 = 1.5$ ms, $\delta_2 = 0.75$ ms. The phase cycling employed is $\phi1 = (x,-x)$; $\phi2 = 2(x),2(-x)$; $\phi3 = 4(x),4(-x)$; $\phi4 = x$; $\phi5 = 8(x),8(-x)$; $\phi6 = x$; rec. = (x,–x,–x,x). Quadrature in F1 is achieved via States-TPPI (Marion et al., 1989) of $\phi2$. For each value of t_2, N- and P-type coherences are obtained by recording data sets where the signs of the gradients g8 and g8' are inverted and 180° is added to the phase $\phi6$. The phase $\phi4$ and the phase of the receiver are incremented by 180° for each increment of t_2. The durations and strengths of the gradients are g1 = (0.5 ms, 8 G/cm), g2 = (0.5 ms, 10 G/cm), g3 = (1.0 ms, 10 G/cm), g4 = (1.0 ms, 6 G/cm), g5 = (0.4 ms, 5 G/cm), g6 = (1.0 ms, 15 G/cm), g7 = (1.0 ms, –10 G/cm), g8' = (1.25 ms, –15 G/cm), g8 = (1.25 ms, 15 G/cm), g9 = (0.3 ms, 1.25 G/cm), g10 = (0.5 ms, 2 G/cm), g11 = (0.125 ms, 29 G/cm).

Sequence (e), HSQC-NOESY-HSQC: ^{13}C$^\alpha$ 180° pulses are applied with the ^{13}C carrier centered at 58 ppm using a 21 kHz field. ^{13}C' decoupling is achieved using a 118 ppm cosine-modulated WALTZ-16 (Shaka et al., 1983) field employing pulses having the SEDUCE-1 (McCoy and Mueller, 1992) profile (330 μs 90° pulses). The delays are as follows: $\tau_a = 2.4$ ms, $\tau_b = 1.5$ ms, $\tau_c = 0.75$ ms. The phase cycling is $\phi1 = (x,-x)$; $\phi2 = 2(x),2(y),2(-x),2(-y)$; $\phi3 = x$; rec. = (x,–x,–x,x). Quadrature in F1 is obtained via States-TPPI (Marion et al., 1989) of $\phi1$. Quadrature in F2 is achieved using the gradient approach described above with the phase $\phi3$ and the sign of the gradient g12 inverted to generate N- and P-type data sets (Kay et al., 1992). The durations and strengths of the gradients are g1 = (1.0 ms, 4 G/cm), g2 = (0.5 ms, 2 G/cm), g3 = (1.0 ms, 15 G/cm), g4 = (0.5 ms, –7 G/cm), g5 = (0.5 ms, 5 G/cm), g6 = (1.0 ms, 8 G/cm), g7 = (0.5 ms, 2 G/cm), g8 = (1.0 ms, 10 G/cm), g9' = (1.25 ms, –15 G/cm), g9 = (1.25 ms, 15 G/cm), g10 = (0.3 ms, 1.25 G/cm), g11 = (0.5 ms, 2 G/cm), g12 = (0.125 ms, 29 G/cm).

poor chemical shift dispersion in ^{1}H and ^{13}C, making conventional 3D and 4D ^{13}C-edited NOESY experiments of very limited use for the assignment of aliphatic-aliphatic NOEs. The following experiments have been developed to overcome this resonance overlap problem.

C_i-NOESY-TOCSY-$N_{j+1}H_{j+1}$ Figure 3a illustrates the pulse scheme for the C$_i$-NOESY-TOCSY-N$_{j+1}$H$_{j+1}$ experiment for detecting aliphatic-aliphatic NOEs. The flow of magnetization transfer in this experiment is described concisely by

$$^{1}HC_i \xrightarrow{J_{CH}} {}^{13}C_i(t_1) \xrightarrow{J_{CH}} {}^{1}HC_i \xrightarrow{NOE} {}^{1}HC_j \xrightarrow{J_{CH}} {}^{13}C_j \xrightarrow{TOCSY} {}^{13}C_j^{\alpha} \xrightarrow{J_{C^{\alpha}C'}} {}^{13}C_j' \xrightarrow{J_{C'N}} {}^{15}N_{j+1}(t_2) \xrightarrow{J_{NH}} {}^{1}HN_{j+1}(t_3) \quad (1)$$

The relevant couplings involved in each of the magnetization transfer steps and the NOE and ^{13}C-^{13}C homonuclear TOCSY transfer periods are indicated above the arrows with the t_1, t_2, t_3 acquisition periods noted in parentheses. Schematic diagrams for the other experiments will use the same labeling. Fourier transformation of the data in each of the three dimensions yields a spectrum with cross peaks at $(\omega_{C_i},\omega_{N_{j+1}},\omega_{HN_{j+1}})$, corresponding to an NOE transfer occurring between a proton of residue i and a proton of residue j located within approximately 5 Å.

The magnetization transfer steps involved in this pulse scheme are straightforward. However, the $^{13}C^{\alpha}$-$^{13}C'$ transfer (via $J_{C^{\alpha}C'}$) deserves comment since evolution due to the passive $^{13}C^{\alpha}$-$^{13}C^{\beta}$ coupling during this period can significantly attenuate the signal. To minimize such magnetization losses, at least three different strategies can be employed. In the first case, the $^{13}C^{\alpha}$-$^{13}C'$ transfer time can be shortened somewhat so that evolution due to the reasonably large (~55 Hz) $^{13}C^{\alpha}$-$^{13}C'$ coupling occurs with only modest interference from the passive $^{13}C^{\alpha}$-$^{13}C^{\beta}$ coupling. However, since a compromise transfer delay must be chosen, complete or near-complete $^{13}C^{\alpha}$-$^{13}C'$ magnetization transfer is not possible. A second strategy involves the use of $^{13}C^{\beta}$ decoupling using frequency swept, B_1 ramped CHIRP pulses (Böhlen et al., 1989) in an analogous manner to the schemes proposed recently by Kupce and coworkers (Kupce and Freeman, 1995; Kupce and Wagner, 1995). It is possible to provide efficient $^{13}C^{\beta}$ decoupling over a bandwidth which covers all residues with the exception of alanine, serine and threonine. It is straightforward to decouple the $^{13}C^{\beta}$ carbons of alanine as well by applying an additional field centered at 15 ppm. In our experience, however, signals from glycine are somewhat attenuated using this procedure, since the decoupling field must be swept sufficiently downfield to affect the $^{13}C^{\beta}$ spins of leucine (~42 ppm). A third approach makes use of 3.6 ms cosine-modulated G3 inversion pulses which invert $^{13}C^{\beta}$ magnetization and hence refocus the effects of this passive coupling, as described by McCoy (1995). Unfortunately, the bandwidth of these pulses does not cover the complete $^{13}C^{\beta}$ chemical shift range, and numerical simulations show that a cosine-modulated G3 inversion pulse inverts magnetization (from M_z to at least $-0.7\ M_z$) over a range of approximately 1 kHz. This profile is sufficient for roughly half of the 20 amino acids. We have recorded spectra using all three different approaches during the course of our studies involving the drkN SH3 domain and Δ131Δ.

The pulse schemes for the C_i-NOESY-TOCSY-$N_{j+1}H_{j+1}$ and (H)C(CO)NH-TOCSY experiment (Montelione et al., 1992; Grzesiek et al., 1993; Logan et al., 1993), used for side-chain aliphatic ^{13}C assignment, are very similar. In fact, peaks observed in (H)C(CO)NH-TOCSY spectra also appear in C_i-NOESY-TOCSY-$N_{j+1}H_{j+1}$ spectra at $(\omega_{C_i},\omega_{N_{i+1}},\omega_{HN_{i+1}})$ due to magnetization which is not transferred via NOE or to intraresidue aliphatic-aliphatic NOEs. Figure 2a illustrates schematically the magnetization transfer pathway in this experiment. Note that the ^{13}C chemical shift(s) (F1) of the carbon(s) attached to the proton(s) in residue i from which the NOE originates and the ^{15}N (F2) and NH (F3) chemical shifts of residue j+1 are recorded. Information regarding residue type and side-chain position for the proton from which the NOE originates ($^{1}HC_i$) can often be inferred from the attached ^{13}C chemical shift in an unfolded protein. Thus, the ^{13}C shift can lead to partial assignment of residue type/position but not sequence-specific assignment for the origination proton. Conversely, information regarding the destination proton is only residue-specific based on the ^{15}N and NH chemical shifts of residue j+1. Because of the reasonable resolution in the nitrogen dimension, assignment of the destination residue is often unambiguous, but there is no information regarding which proton in this residue serves as acceptor of the magnetization. This is the result of the carbon TOCSY period which mixes magnetization from all aliphatic carbons of a particular residue and prevents site-specific assignment. Additional information regarding the residue where magnetization originates and the side-chain position for the destination proton may be obtained for an NOE at $(\omega_{C_i},\omega_{N_{j+1}},\omega_{HN_{j+1}})$ from the symmetry-related cross peak at $(\omega_{C_j},\omega_{N_{i+1}},\omega_{HN_{i+1}})$. Note that because of differential relaxation times associated with spins in residues i and j and the different transfer functions (Bax et al., 1990) that describe the efficiency of TOCSY magnetization transfers to the $^{13}C^{\alpha}$ positions of residues i and j, the symmetry-related peaks will likely not be of the same intensity. Although the information content of this experiment is, in general, insufficient to allow the complete site-specific description of an NOE, it is nonetheless very useful. This is particularly the case considering that specific atomic interactions may be less important in unfolded states or partially folded states than in folded molecules. In addition, the goal of structural characterization of unfolded states is modest compared to that for folded proteins. It should also be noted that the use of the ^{15}N and NH resonances limits the available NOEs to those for which the destination residue does not precede proline. Thus, symmetry-related peaks can only be observed if both residues do not precede proline.

Figure 4a demonstrates the application of this pulse scheme to Δ131Δ. The strip plot at the ^{1}H (F3) and ^{15}N (F2) chemical shifts of Val^{114} shows the C^{α} and C^{β} resonances of the preceding residue, Tyr^{113}, as 'auto' peaks

(also seen in the (H)C(CO)NH-TOCSY spectrum in Fig. 4b). There are several additional peaks which can be unambiguously assigned to sequential and short-range NOEs to either the $^1H^{\alpha}$ or $^1H^{\beta}$ of Tyr^{113}. The assignments of the protons from which magnetization originates in the NOE transfer are indicated on the left-hand side of each of the cross peaks. These assignments are facilitated by the presence of symmetry-related peaks, as described in the next paragraph. For two peaks at the carbon chemical shifts of 24.8 and 28.7 ppm, which correspond to the γ and δ shifts of a lysine residue, symmetry-related peaks were not found and therefore residue-specific assignments of these NOEs could not be established. In Figs. 4c and d, 2D slices from the simultaneous $^{15}N,^{13}C$-edited 3D NOESY experiment are shown. These slices are taken at the $^{13}C^{\alpha}$ and $^{13}C^{\beta}$ chemical shifts of Tyr^{113}, respectively, and the H^{α} and H^{β} shifts of Tyr^{113} are indicated by arrows in the figure. Although there are many NOE peaks observed in these slices, several other tyrosine residues in the protein have nearly degenerate ^{13}C and ^1H resonances, making the assignment of these NOEs impossible. The resolving power of the C_i-NOESY-TOCSY-$N_{j+1}H_{j+1}$ experiment relative to the conventional ^{13}C-edited 3D NOESY experiment is clear.

The utility of symmetry-related cross peaks for the site-specific assignment of the origination protons (^1HC_i, in transfer scheme 1) is shown in Fig. 5. Strip plots taken at the ^1H (F3) and ^{15}N (F2) chemical shifts of residues Asp^{83}, Gly^{88}, Leu^{89} and Ala^{90} demonstrate NOEs to aliphatic side chains of Thr^{82}, Arg^{87}, Gly^{88} and Leu^{89}, respectively. In particular, symmetry-related NOEs demonstrating interactions of Gly^{88} with Thr^{82}, Arg^{87} and Leu^{89} are shown. The long-range (i,i+6) NOEs from Thr^{82} to Gly^{88} are especially noteworthy. These NOEs are reflected in the figure by appearances of a peak at the chemical shift of the $^{13}C^{\alpha}$ of Gly^{88} and the (^{15}N,NH) shifts of Asp^{83} and two peaks at the chemical shifts of the α and γ2 carbons of Thr^{82} and the (^{15}N,NH) shifts of Leu^{89}. In this case we can establish that the NOEs involve the α protons of Gly^{88} and the α and γ2 protons of Thr^{82}, but not the β proton of Thr^{82}.

C_i-NOESY-$N_{j+1}H_{j+1}$ It is particularly helpful to obtain specific NOE information involving α protons in order to identify the secondary structure in partially folded proteins. The short-range $d_{\alpha\beta}(i,i+3)$ and $d_{\alpha\alpha}(i,j)$ NOEs are

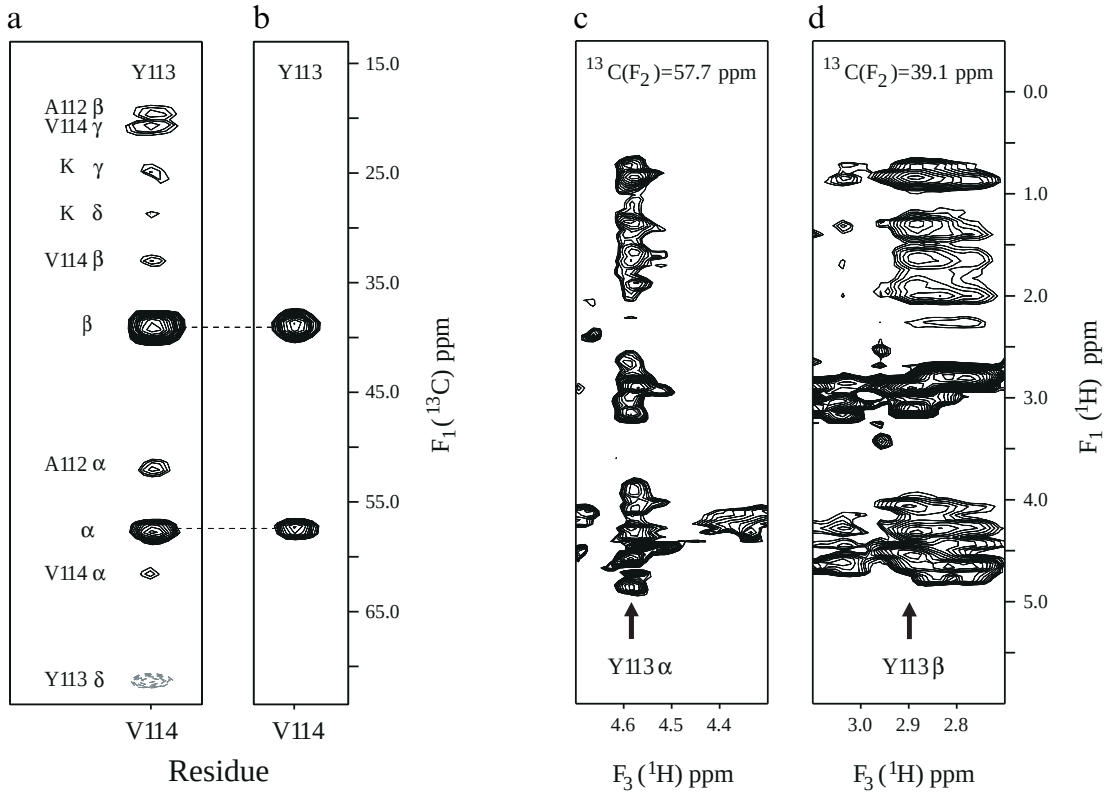

Fig. 4. Strip plots from the 3D C_i-NOESY-TOCSY-$N_{j+1}H_{j+1}$ spectrum (a) (200 ms mixing time, 600 MHz, ^1H frequency) and the corresponding 3D (H)C(CO)NH-TOCSY spectrum (b) (600 MHz, ^1H frequency) at the ^{15}N and NH chemical shifts of Val^{114} of Δ131Δ. The auto peaks in the NOESY experiment at ($^{13}C_i$,$^{15}N_{i+1}$,NH_{i+1}) of Tyr^{113} are labeled as α, β and are the only peaks observed in the (H)C(CO)NH-TOCSY. NOEs from other residues to Tyr^{113} are labeled by residue and side-chain position. The peak at the ^{13}C chemical shift of 71.6 ppm is folded and corresponds to an intraresidue NOE from Tyr^{113} δ to one or more aliphatic protons. ($^{13}C^{\beta}$ decoupling was not utilized.) (c) and (d) 2D slices from a simultaneous 3D $^{13}C,^{15}N$-NOESY data set (200 ms mixing time, 500 MHz, ^1H frequency) showing NOEs to the H^{α} and H^{β} of Tyr^{113}. The slices were taken at the carbon shifts of Tyr^{113} C^{α} (57.7 ppm) and C^{β} (39.1 ppm), respectively. Arrows point to the Tyr^{113} H^{α} (4.58 ppm) and H^{β} (2.90 ppm) chemical shifts in the F3 dimension.

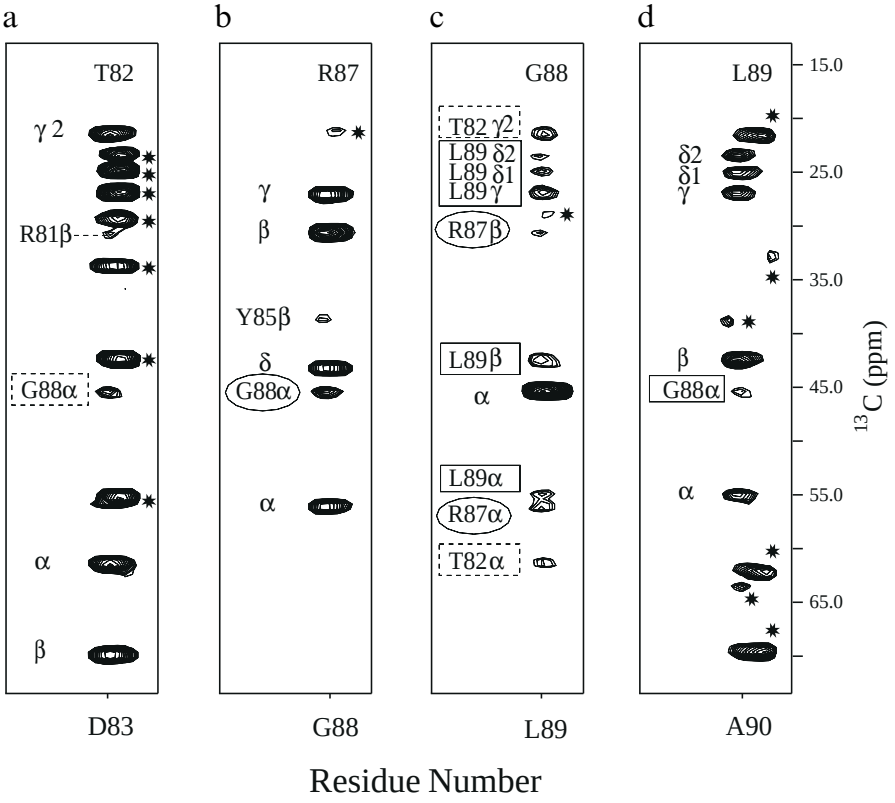

Fig. 5. Strip plots from the 3D C_i-NOESY-TOCSY-$N_{j+1}H_{j+1}$ spectrum (200 ms mixing time, 600 MHz, ^{1}H frequency) at the ^{15}N and NH chemical shifts of Asp[83] (a), Gly[88] (b), Leu[89] (c) and Ala[90] (d) of Δ131Δ highlighting the symmetry-related NOE peaks involving side-chain protons of Thr[82], Arg[87], Gly[88] and Leu[89], indicated at the top of these panels. Auto peaks at ($^{13}C_i$,$^{15}N_{i+1}$,NH_{i+1}) are labeled as α, β, γ, etc. NOE peaks are labeled with the residue and side-chain position corresponding to the origination site of magnetization and with the destination residue named at the top of the panels. In particular, three NOE peaks labeled within dotted rectangles in panels (a) and (c) correspond to symmetry-related NOEs between Thr[82] and Gly[88]. NOEs labeled within ovals in panels (b) and (c) are symmetry-related and correspond to magnetization transfer between Arg[87] and Gly[88], and five symmetry-related NOE pairs between Gly[88] and Leu[89] are labeled with solid rectangles in panels (c) and (d). Peaks labeled with an asterisk are from unrelated residues having similar ^{15}N and NH chemical shifts.

characteristic of α-helix and β-sheets, respectively. Although, in principle, NOE information between neighboring α protons is available in the C_i-NOESY-TOCSY-$N_{j+1}H_{j+1}$ experiment, in most cases it is not possible to establish with certainty the identity of the protons involved in the NOE transfer. For this reason and for sensitivity considerations, it is preferable to omit the TOCSY transfer period in the sequence of Fig. 3a when H^α-H^α and other aliphatic protons to H^α NOEs are sought (see Fig. 3a.1). In this case, only NOEs between two α protons will have symmetry-related peaks, enabling the sequence-specific identification of both origination and destination residues. However, quite often NOEs from other aliphatic protons can be assigned as well. In the case of Δ131Δ we have observed a number of $d_{\alpha\beta}(i,i+3)$ NOEs in regions of the molecule that are helical in wild-type staphylococcal nuclease (Loll and Lattman, 1989). Data recorded with the C_i-NOESY-$N_{j+1}H_{j+1}$ pulse scheme on the folded form of staphylococcal nuclease are presented later (see below).

Both C_i-NOESY-TOCSY-$N_{j+1}H_{j+1}$ and C_i-NOESY-$N_{j+1}H_{j+1}$ label the site from which magnetization originates by the carbon chemical shift. However, difficulties may still exist in assigning these carbon resonances to specific residues because of the degeneracy of aliphatic carbon chemical shifts in general and the possible disappearance of symmetry-related peaks due to different relaxation rates associated with each transfer pathway and poor transfer efficiencies in some cases. Additionally, NOE peaks between two side chains of the same residue type will often be indistinguishable from auto peaks due to the degeneracy of carbon chemical shifts. In principle, by recording the ^{15}N chemical shifts of residues immediately following both the origination and destination residues, it is possible to resolve many of the ambiguities that arise. However, such a scheme requires two carbon isotropic mixing periods to transfer aliphatic magnetization to and from the backbone if NOEs involving side-chain aliphatic protons are to be observed. The sensitivity of this experiment for both the drkN SH3 domain and Δ131Δ samples was insufficient to yield information of real use.

N_{i+1}-NOESY-$N_{j+1}H_{j+1}$ This experiment allows the detection of NOEs between the α protons of residues i and j. The magnetization transfer steps involved in the

experiment are indicated schematically in Fig. 2b and the pulse scheme employed is illustrated in Fig. 3b. The flow of magnetization transfer is described by

$$^{1}HN_{i+1} \xrightarrow{J_{NH}} {}^{15}N_{i+1}(t_1) \xrightarrow{J_{C'N}} {}^{13}C'_i \xrightarrow{J_{C^\alpha C'}} {}^{13}C^\alpha_i \xrightarrow{J_{CH}} {}^{1}HC^\alpha_i \xrightarrow{NOE} {}^{1}HC^\alpha_j \xrightarrow{J_{CH}} {}^{13}C^\alpha_j \xrightarrow{J_{C^\alpha C'}} {}^{13}C'_j \xrightarrow{J_{C'N}} {}^{15}N_{j+1}(t_2) \xrightarrow{J_{NH}} {}^{1}HN_{j+1}(t_3) \quad (2)$$

Note that magnetization is transferred from $^{1}HN_{i+1}$ to $^{1}HC^\alpha_i$ and from $^{1}HC^\alpha_j$ to $^{1}HN_{j+1}$ using HNCO-type (Kay et al., 1990) transfer steps. Immediately after the transfer of magnetization from $^{13}C'_i$ to $^{13}C^\alpha_i$, the $^{13}C^\alpha$ magnetization is antiphase with respect to the coupled carbonyl spin and must be refocused prior to additional transfer steps. Evolution due to the passive $^{13}C^\alpha$-$^{13}C^\beta$ coupling which occurs during this transfer period can be refocused using one of a number of strategies for $^{13}C^\beta$ decoupling described above for the C_i-NOESY-TOCSY-$N_{j+1}H_{j+1}$ experiment.

The N_{i+1}-NOESY-$N_{j+1}H_{j+1}$ experiment provides NOE cross peaks at ($\omega_{N_{i+1}}$,$\omega_{N_{j+1}}$,$\omega_{HN_{j+1}}$) and symmetry-related peaks at ($\omega_{N_{j+1}}$,$\omega_{N_{i+1}}$,$\omega_{HN_{i+1}}$) connecting the H^α protons of residues i and j. Information will be missing where the residues of interest precede proline. The application of this scheme to Δ131Δ is illustrated in Fig. 6, where a strip plot at the ^{1}H (F3) and ^{15}N (F2) chemical shifts of Gly[50] is shown. The auto peak corresponding to magnetization residing on the H^α of Lys[49] both before and after the mixing period appears at the ^{15}N chemical shift of Gly[50] in F1. NOEs between the α protons of Lys[48] and Lys[49] and between Lys[49] and Gly[50] are observed and can be readily assigned since symmetry-related peaks for each of these two NOEs are observed as well (data not shown).

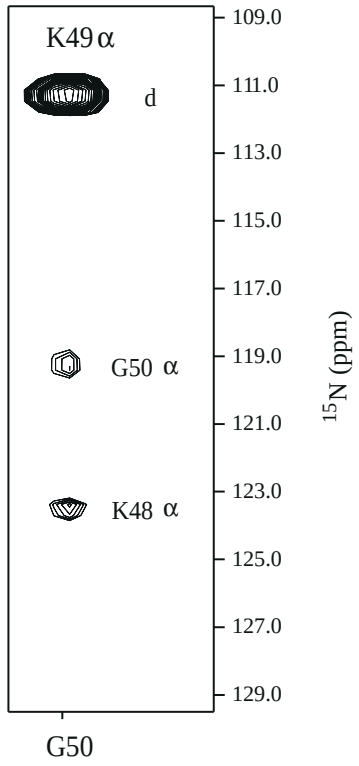

Fig. 6. Strip plot from the 3D N_{i+1}-NOESY-$N_{j+1}H_{j+1}$ spectrum (200 ms mixing time, 500 MHz, ^{1}H frequency) at the ^{15}N and NH chemical shifts of Gly[50] of Δ131Δ. Sequential NOEs between the H^α protons of Lys[48] and Lys[49] (labeled as K48 α) and between Gly[50] and Lys[49] (labeled as G50 α) are observed at the ^{15}N chemical shifts (F1) of Lys[49] and Val[51], respectively. The auto peak is labeled as d. ($^{13}C^\beta$ decoupling was employed with cosine-modulated G3 pulses.)

It is not possible to unambiguously assign all of the NOEs in this Δ131Δ data set because of the degeneracy of ^{15}N chemical shifts and the absence of some symmetry-related peaks. A simple modification to this pulse scheme can be made whereby the chemical shift of the carbonyl carbon of residue i, rather than the ^{15}N shift of residue i+1, is recorded. Figure 1 illustrates that there is reasonable C' chemical shift dispersion in unfolded proteins that can be exploited for NOE assignment. Figure 3b.1 illustrates the modifications to the pulse scheme allowing recording of the C' shift.

Aliphatic-NH NOEs

N_{i+1}-TOCSY-NOESY-N_jH_j A 3D ^{15}N-edited NOESY data set is commonly used to probe aliphatic-NH NOEs. However, medium- or long-range NOEs which are generally weaker than sequential NOEs may escape detection due to resonance overlap with sequential NOE cross peaks. Figure 2c illustrates schematically the transfer steps in the N_{i+1}-TOCSY-NOESY-N_jH_j experiment, which has been developed to provide better resolution of aliphatic-NH NOEs, and the pulse scheme is indicated in Fig. 3c. The flow of magnetization in this experiment can be described succinctly as follows:

$$^{1}HN_{i+1} \xrightarrow{J_{NH}} {}^{15}N_{i+1}(t_1) \xrightarrow{J_{C'N}} {}^{13}C'_i \xrightarrow{J_{C^\alpha C'}} {}^{13}C^\alpha_i \xrightarrow{TOCSY} {}^{13}C_i \xrightarrow{J_{CH}} {}^{1}HC_i \xrightarrow{NOE} {}^{1}HN_j \xrightarrow{J_{NH}} {}^{15}N_j(t_2) \xrightarrow{J_{NH}} {}^{1}HN_j(t_3) \quad (3)$$

NOEs connecting the aliphatic protons of residue i to the NH of residue j are obtained and the ^{15}N (F1) chemical shift of residue i+1 and the ^{15}N (F2) and NH (F3) chemical shifts of residue j are recorded, as illustrated in Fig. 2c. Thus, cross peaks are observed at ($\omega_{N_{i+1}}$,ω_{N_j},ω_{HN_j}). Note that it is not possible to establish which proton on residue i is responsible for the NOE to the NH of residue j. In addition, because NOEs are selected from aliphatic protons to NH, symmetry-related peaks are not generated in this experiment.

The utility of this scheme is illustrated in Fig. 7a, where a strip plot at the ^{15}N and NH chemical shifts of Gly[79] of Δ131Δ is shown. In this case, NOEs from aliphatic protons of Lys[78] and Asn[77], recorded at the ^{15}N chemical shifts (F1) of Gly[79] and Lys[78], respectively, are observed. In addition, an intraresidue NOE connecting

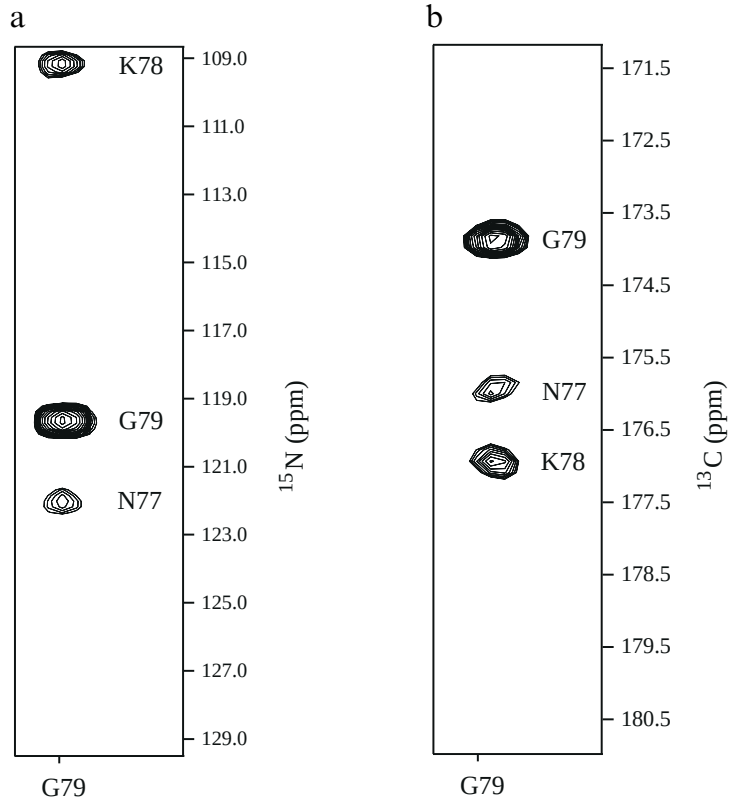

Fig. 7. (a) Strip plot from the 3D N_{i+1}-TOCSY-NOESY-N_jH_j spectrum (200 ms mixing time, 500 MHz, ^{1}H frequency) at the ^{15}N and NH chemical shifts of Gly^{79} of Δ131Δ. The three well-resolved peaks observed at the ^{15}N chemical shifts of Lys^{78}, Gly^{79} and Gln^{80} in F1 correspond to NOEs from the aliphatic side-chain protons of Asn^{77}, Lys^{78} and Gly^{79} to the NH of Gly^{79}. (b) Strip plot from the 3D (HN)CO_i-TOCSY-NOESY-N_jH_j spectrum (200 ms mixing time, 500 MHz, ^{1}H frequency) at the ^{15}N and NH chemical shifts of Gly^{79} of Δ131Δ. The three well-resolved peaks observed at the ^{13}C' chemical shifts of Asn^{77}, Lys^{78} and Gly^{79} in F1 correspond to NOEs from the aliphatic side-chain protons of Asn^{77}, Lys^{78} and Gly^{79} to the NH of Gly^{79}. (This experiment and the experiment in (a) employed $^{13}C^{\beta}$ decoupling using cosine-modulated G3 pulses.)

the H^{α} and NH protons of Gly^{79} is recorded at the ^{15}N chemical shift (F1) of Gln^{80}. In order to unambiguously assign the NOEs in this experiment, the ^{15}N chemical shift recorded in F1 must be unique. In most cases, several residues will share identical or very similar ^{15}N chemical shifts and additional information regarding the site of origination of the magnetization will be required for an unambiguous assignment. This is the case for the NOEs illustrated in Fig. 7a, which could only be definitively assigned by making use of an experiment which substitutes the recording of the ^{15}N chemical shift of residue i+1 with the C' shift of residue i, as described below.

(HN)CO_i-TOCSY-NOESY-N_jH_j The (HN)CO_i-TOCSY-NOESY-N_jH_j experiment is almost identical to the N_{i+1}-TOCSY-NOESY-N_jH_j experiment, with only a difference in t_1 chemical shift evolution periods (see Fig. 3c.1). Thus, cross peaks at ($\omega_{C'_i}$,ω_{N_j},ω_{HN_j}) rather than ($\omega_{N_{i+1}}$,ω_{N_j},ω_{HN_j}) are observed. The application of this pulse scheme to Δ131Δ is shown in Fig. 7b with a strip plot at the ^{15}N and NH chemical shifts of Gly^{79}. The combination of the ^{15}N chemical shift of residue i+1 and the ^{13}C' chemical shift of residue i allows the unambiguous assignment of the three NOEs illustrated in Figs. 7a and b. Again, because of the isotropic mixing period, observed NOEs only provide information on the proximity of a particular NH to some or all of the aliphatic protons of a given residue, but not to a specific side-chain proton.

N_{i+1}-NOESY-N_jH_j The observation of H^{α}-NH NOEs is critical for the identification of preferential sampling of specific backbone conformations. The sequential $d_{\alpha N}$(i,i+1) and intraresidue $d_{\alpha N}$(i,i) distances are always less than 3.6 Å, giving rise to relatively strong NOEs throughout the entire sequence. Short- and medium-range $d_{\alpha N}$(i,i+2) to $d_{\alpha N}$(i,i+4) or longer range NOEs, however, provide evidence for particular structural preferences. The smaller magnitude of these short- and medium-range NOEs relative to sequential and intraresidue NOEs coupled with the very small α proton chemical shift dispersion in unfolded proteins makes their analysis extremely difficult using conventional ^{15}N-edited NOESY experiments. In our approach, the assignment of $d_{\alpha N}$(i,j) NOEs can be achieved by omitting the TOCSY mixing period in the scheme of Fig. 3c (see Fig. 3c.2), thereby ensuring that the magnetization of interest resides on the H^{α} spins immediately prior to NOE mixing. In comparison to the N_{i+1}-TOCSY-NOESY-N_jH_j scheme, the present experiment yields specific H^{α}-NH NOEs and these NOEs are observed with higher sensitivity due to the removal of the

carbon TOCSY transfer step (see Fig. 3c). Note that the direction of magnetization transfer is one-way, H^{α} to NH, and therefore symmetry-related cross peaks are not observed with this pulse scheme. Cross peaks connecting the H^{α} of residue i with the NH of residue j are observed at $(\omega_{N_{i+1}},\omega_{N_j},\omega_{HN_j})$.

Figure 8a shows the application of the N_{i+1}-NOESY-N_jH_j experiment to Δ131Δ. A strip plot at the ^{15}N (F2) and NH (F3) chemical shifts of Leu[108] shows the sequential NOE between the α protons of Gly[107] and the NH of Leu[108] observed at the ^{15}N chemical shift of Leu[108] in F1. The intraresidue H^{α}-NH NOE of Leu[108] is observed at the ^{15}N chemical shift (F1) of Ala[109]. Strong sequential and intraresidue $d_{\alpha N}(i,i+1)$ and $d_{\alpha N}(i,i)$ NOEs are ubiquitous in spectra of the unfolded states of both drkN SH3 and Δ131Δ. Therefore, this information can be used to facilitate sequential assignment, in a similar approach to the NOE-based strategy used for the sequential assignment of small folded proteins (Wüthrich, 1986). The unambiguous assignment of NOE peaks is, however, best ensured by using a combination of data from the N_{i+1}-NOESY-N_jH_j experiment and from experiments where the backbone carbonyl chemical shift of residue i is recorded in place of the ^{15}N shift of residue i+1, such as in the (HN)CO_i-NOESY-N_jH_j experiment recorded by incorporating both the (c.1) and (c.2) substitutions into the pulse scheme in Fig. 3c or the (HCA)CO_i-NOESY-N_jH_j experiment described below.

(HCA)CO_i-NOESY-N_jH_j At least two strategies are available for recording the C' chemical shift of the residue from which magnetization originates in a NOESY transfer between H^{α} and NH spins. The first approach makes use of an HNCO-type sequence (Kay et al., 1990), while the second employs an HCACO transfer (Kay et al., 1990). The flow of magnetization in the (HCA)CO_i-NOESY-N_jH_j pulse scheme is indicated in Fig. 2d and the sequence utilized is illustrated in Fig. 3d. Briefly, the coherence transfer steps in this experiment can be described as follows:

$$\begin{aligned} &{}^{1}H_i^{\alpha} \xrightarrow{J_{CH}} {}^{13}C_i^{\alpha} \xrightarrow{J_{C^{\alpha}C'}} {}^{13}C_i'(t_1) \xrightarrow{J_{C^{\alpha}C'}} \\ &{}^{13}C_i^{\alpha} \xrightarrow{J_{C^{\alpha}H}} {}^{1}HC_i^{\alpha} \xrightarrow{NOE} {}^{1}HN_j \xrightarrow{J_{NH}} \\ &{}^{15}N_j(t_2) \xrightarrow{J_{NH}} {}^{1}HN_j(t_3) \end{aligned} \qquad (4)$$

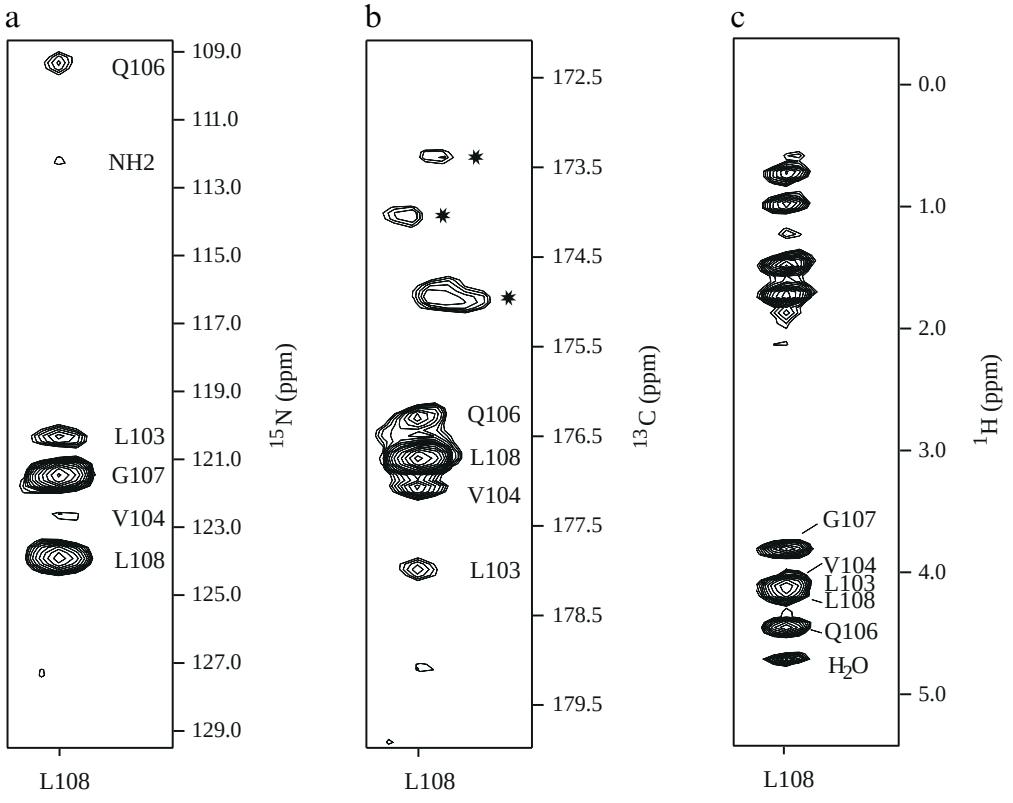

Fig. 8. (a) Strip plot from the 3D N_{i+1}-NOESY-N_jH_j spectrum (200 ms mixing time, 500 MHz, ^{1}H frequency) taken at the ^{15}N and NH chemical shifts of Leu[108] of Δ131Δ. The six well-resolved peaks correspond to NOEs from the α protons of Leu[103], Val[104], Gln[106], Gly[107] and Leu[108] and from the β or γ protons of an unknown asparagine or glutamine residue (labeled as NH2) to the NH of Leu[108]. ($^{13}C^{\beta}$ decoupling was achieved using cosine-modulated G3 pulses.) (b) Strip plot from the 3D (HCA)CO_i-NOESY-N_jH_j spectrum (200 ms mixing time, 500 MHz, ^{1}H frequency) taken at the ^{15}N and NH chemical shifts of Leu[108] of Δ131Δ. The peaks labeled with asterisks are associated with a residue having nearby ^{15}N and NH chemical shifts. Note that the NOE involving the H^{α} protons of Gly[107] is not observed since the (HCA)CO transfer in this pulse scheme severely attenuates methylene groups. ($^{13}C^{\beta}$ decoupling was achieved using cosine-modulated G3 pulses.) (c) Strip plot from the ^{15}N-edited NOESY-HSQC spectrum (200 ms mixing time, 500 MHz, ^{1}H frequency) showing NOE contacts to Leu[108]. The plot demonstrates the ambiguities in the assignment of NOEs from the α protons of Val[104], Leu[103] and Leu[108] to the NH of Leu[108].

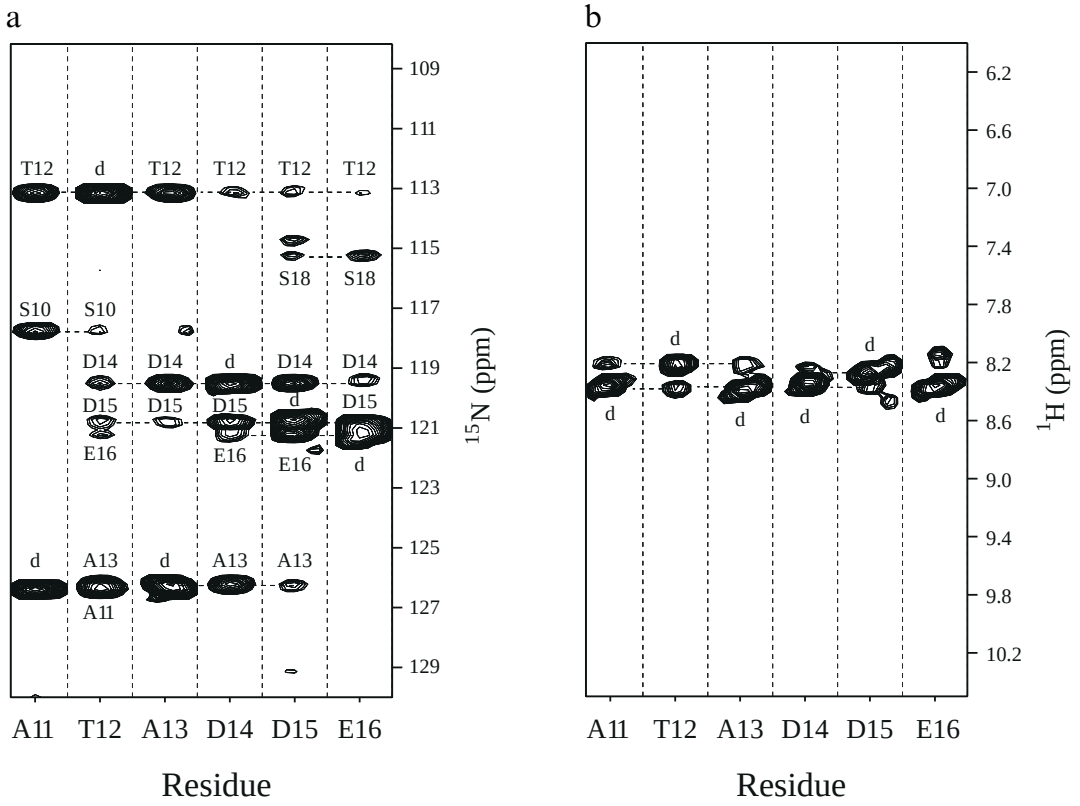

Fig. 9. (a) Strip plot from the 3D ^{15}N-HSQC-NOESY-HSQC spectrum (250 ms mixing time, 600 MHz, ^{1}H frequency) for residues Ala^{11}–Glu^{16} of the unfolded state of the drkN SH3 domain. Auto peaks are labeled as d and the NOE peaks are labeled with the site of origination of magnetization. (b) Strip plot from the 3D ^{15}N-edited NOESY-HSQC spectrum (250 ms mixing time, 500 MHz, ^{1}H frequency) for the same residues. Medium- or long-range NOEs are difficult to assign due to the poor dispersion in the NH region.

Note that it is possible to insert a TOCSY mixing scheme in the sequence, although we did not record such an experiment for the present study. An NOE between the α proton of residue i and the NH of residue j will appear at (ω_{C_i},ω_{N_j},ω_{HN_j}).

The (HCA)CO$_i$-NOESY-N$_j$H$_j$ experiment has a number of advantages relative to the (HN)CO$_i$-NOESY-N$_j$H$_j$ scheme. First, the HCACO transfer is more sensitive than the HNCO approach, at least for approximately 90% of the NOEs observed in the Δ131Δ fragment studied here. Second, the HCACO-based experiment allows the detection of NOEs from protons of residues preceding proline unlike the (HN)CO$_i$-NOESY-N$_j$H$_j$ scheme, where magnetization originates on the NH of residue i+1. However, NOEs from either or both of the two α protons of glycine residues will be greatly attenuated in the present version of this experiment which is optimized for AX spin systems. Similarly, NOEs involving β or γ protons of Asx and Glx residues, respectively, which could potentially be observed due to the HCCO transfer involving the side-chain carbonyl, will also be severely attenuated. As with the other experiments described for detecting aliphatic proton-NH NOEs, symmetry-related peaks are not observed.

The application of the (HCA)CO$_i$-NOESY-N$_j$H$_j$ experiment to Δ131Δ is shown in Fig. 8b with a strip plot at the ^{15}N and NH chemical shifts of Leu^{108}. Comparison with the strip plot from the N$_{i+1}$-NOESY-N$_j$H$_j$ experiment, illustrated in Fig. 8a, enables the unambiguous assignment of the NOEs between the α protons of Leu^{103}, Val^{104} and Gln^{106} and the NH of Leu^{108}. As explained above, the sequential NOEs from the α protons of Gly^{107} to the NH of Leu^{108} are greatly attenuated in the HCACO-based version of the experiment and are not observed in Fig. 8b. The corresponding strip plot from the ^{15}N-edited NOESY at the ^{15}N and NH chemical shifts of Leu^{108} is shown in Fig. 8c, demonstrating the overlap of the α proton chemical shifts of Leu^{103}, Val^{104} and Leu^{108}. Since sequential and intraresidue NOEs are always strong and present, the weaker and longer range NOEs which provide more structural information, such as the NOEs involving the H$^{\alpha}$s of Leu^{103} and Val^{104}, may well be overlooked in the ^{15}N-edited NOESY.

As discussed above, the N$_{i+1}$-TOCSY-NOESY-N$_j$H$_j$ and N$_{i+1}$-NOESY-N$_j$H$_j$ experiments provide NOEs connecting the aliphatic (TOCSY-NOESY) and H$^{\alpha}$ (NOESY) protons of residue i with the NH protons of residue j. Ambiguities in the assignment of NOEs caused by the degeneracy of the ^{15}N chemical shifts can be overcome by recording the C' chemical shift of residue i rather than the nitrogen shift of residue i+1. An alternative strategy is based

on reversing the flow of magnetization in the N_{i+1}-TOCSY-NOESY-N_jH_j and N_{i+1}-NOESY-N_jH_j experiments. This can be achieved by recording the ^{15}N shift of residue j prior to an NOE mixing period where magnetization from NH_j is transferred to nearby protons. Subsequently, magnetization on H_i^{α} (note that a carbon TOCSY period can be inserted to transfer a signal from H_i^{ali} to H_i^{α}) can be relayed to the ^{15}N and NH spins of residue i+1 via an H(CACO)NH-type experiment. In this way NOEs from NH_j to H_i^{ali} or H_i^{α} can be detected at $(\omega_{N_j},\omega_{N_{i+1}},\omega_{HN_{i+1}})$. While these experiments have not been implemented in the current study, they would provide symmetry peaks relative to peaks observed in the N_{i+1}-TOCSY-NOESY-N_jH_j and N_{i+1}-NOESY-N_jH_j experiments.

NH-NH NOEs

HSQC-NOESY-HSQC The HSQC-NOESY-HSQC experiment has been described previously and is used for the detection of NH-NH NOEs, particularly in α-helical regions of proteins where the NH chemical shift dispersion is poor (Frenkiel et al., 1990; Ikura et al., 1990) and in proteins deuterated in the aliphatic and aromatic positions where NOEs between NH protons are useful in the calculation of an overall fold of the polypeptide backbone (Grzesiek et al., 1995; Venters et al., 1995). Although the pulse sequence was proposed a few years ago, we have made a number of improvements to the original scheme and, for completeness, the sensitivity-enhanced version used in our laboratory is presented in Fig. 3e. The flow of magnetization is described as follows:

$$\begin{aligned} {}^1HN_i &\xrightarrow{J_{NH}} {}^{15}N_i(t_1) \xrightarrow{J_{NH}} {}^1HN_i \xrightarrow{NOE} \\ {}^1HN_j &\xrightarrow{J_{NH}} {}^{15}N_j(t_2) \xrightarrow{J_{NH}} {}^1HN_j(t_3) \end{aligned} \qquad (5)$$

The observation of symmetry-related NOE cross peaks at $(\omega_{N_i},\omega_{N_j},\omega_{HN_j})$ and $(\omega_{N_j},\omega_{N_i},\omega_{HN_i})$ is extremely useful for resolving ambiguities due to any possible degeneracy of ^{15}N chemical shifts. In addition, because sequential NH-NH NOEs are nearly ubiquitous in an unfolded protein, the method is also very useful for sequential assignment, especially for sequences involving repeats of residues. For

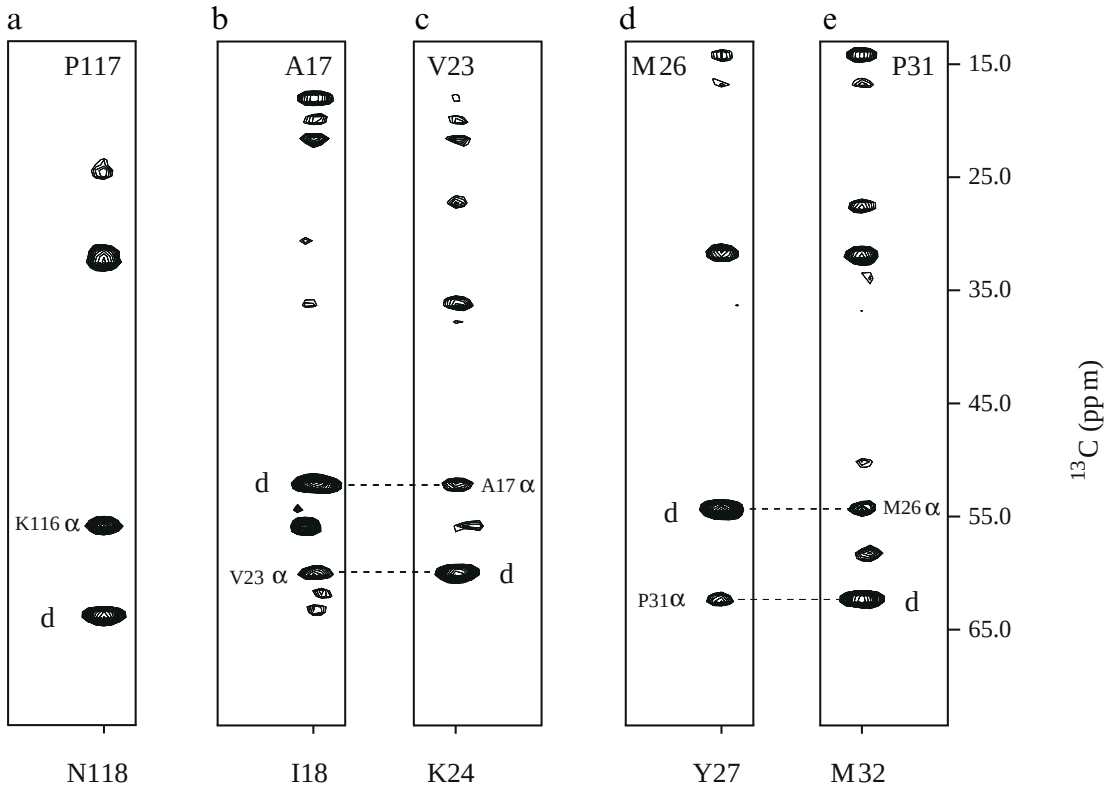

Fig. 10. Strip plots from the 3D C_i-NOESY-$N_{j+1}H_{j+1}$ spectrum (75 ms mixing time, 500 MHz, ^1H frequency) of folded staphylococcal nuclease complexed with pdTp and Ca^{2+}. (In this experiment $^{13}C^{\beta}$ decoupling was achieved using the scheme based on CHIRP pulses.) (a) Strip plot at the ^{15}N and NH chemical shifts of Asn^{118}. The auto peak of Pro^{117} ($^{13}C_i^{\alpha}$,$^{15}N_{i+1}$, NH_{i+1}) is labeled as d. The strong sequential NOE between the H^{α} protons of Lys^{116} and Pro^{117}, labeled as K116 α, demonstrates that these protons are in close proximity, consistent with the cis configuration of the Lys^{116}–Pro^{117} peptide bond. (b) and (c) Strip plots at the ^{15}N and NH chemical shifts of Ile^{18} and Lys^{24}, respectively. The auto peaks of Ala^{17} and Val^{23} are labeled as d. Symmetry-related NOEs between the H^{α} protons of Ala^{17} and Val^{23} are labeled as V23 α and A17 α in panels (b) and (c), respectively. The chemical shift of the H^{α} of Val^{23} is almost identical to the water shift (4.65 ppm). (d) and (e) Strip plots at the ^{15}N and NH chemical shifts of Tyr^{27} and Met^{32}, respectively. The auto peaks of Met^{26} and Pro^{31} are labeled as d. NOEs between the nearly degenerate H^{α} protons of Met^{26} (4.88 ppm) and Pro^{31} (4.86 ppm) are labeled as P31 α and M26 α in panels (d) and (e), respectively.

instance, in Δ131Δ, where several lysine-lysine segments appear in the protein sequence, data from the HSQC-NOESY-HSQC experiment were invaluable in allowing the completion of the sequential assignment.

Figure 9 demonstrates the resolving power of this experiment for the identification of NH-NH NOEs in the drkN SH3 domain. Strips from the ^{15}N and NH chemical shifts of Ala^{11}–Glu^{16} are shown in Fig. 9a. Strong sequential NOEs are clearly present for all residues here. More interesting are the medium-range NH-NH NOEs, including Ser^{10}–Thr^{12}, Thr^{12}–Asp^{14}, Ala^{13}–Asp^{15}, Thr^{12}–Asp^{15} and Thr^{12}–Glu^{16} NOEs. The symmetric nature of the NOEs observed in this experiment allows confirmation of these assignments. Recalling that this protein is in slow exchange between its unfolded and folded states, it is worth noting that, for the corresponding folded state, (i,i+1) and (i,i+2) NH-NH NOEs only are observed in this region, making it unlikely that the (i,i+3) and (i,i+4) NOEs observed in the unfolded state are the result of either exchange or spin diffusion. For comparison, strip plots from the ^{15}N-edited NOESY experiment for the same residues are shown in Fig. 9b. While the ^{15}N-edited NOESY has intrinsically higher sensitivity, only a very limited number of unambiguous assignments can be made from these data.

Application to folded proteins

It is clear that a number of the experiments described above in the context of structural studies of unfolded and partially folded proteins are well suited for application to folded molecules as well. For example, the HSQC-NOESY-HSQC experiment was originally developed to assist in the assignment of NOEs between degenerate NH pairs in folded proteins by recording chemical shifts of the heteronuclei directly coupled to the amide protons. The C_i-NOESY-$N_{j+1}H_{j+1}$ experiment which provides NOEs linking aliphatic/aromatic (i) and H^α (j) protons at (ω_{C_i}, $\omega_{N_{j+1}}$,$\omega_{HN_{j+1}}$) is particularly useful for the assignment of NOEs between degenerate H^α protons or NOEs involving H^α spins that resonate in proximity to water. The assignment of NOEs between degenerate H^α protons can be difficult using conventional 3D ^{13}C-edited NOESY spectroscopy because of overlap with diagonal peaks, and recourse to 4D ^{13}C-NOESY experiments is necessary. The C_i-NOESY-$N_{j+1}H_{j+1}$ experiment offers a simple solution to the problem and, in addition, has the advantage that the experiment is performed on a sample dissolved in H_2O.

The C_i-NOESY-$N_{j+1}H_{j+1}$ experiment described here also provides a simple approach for distinguishing between cis and trans peptide bond configurations. A number of different strategies currently exist for the identification of cis or trans Xaa-Pro peptide bonds. Chazin et al. (1989) have identified populations of both the cis and trans forms of the Gly^{42}–Pro^{43} peptide bond in calbindin D_{9k} on the basis of NOESY cross peaks connecting the H^α protons of Gly^{42} to either the H^α or the H^δ protons of Pro^{43}. A second approach makes use of the 3 ppm upfield shift of the $^{13}C^\gamma$ resonance of proline residues in the cis configuration relative to trans (Torchia, 1984). Recently, Markley and co-workers have developed a general method for the configurational analysis of Xaa-Pro peptide bonds in proteins involving the selective incorporation of either [$^{13}C^\alpha$]Xaa and [$^{13}C^\alpha$]Pro or [$^{13}C^\alpha$]Xaa and [$^{13}C^\delta$]Pro (Hinck et al., 1993). The identification of symmetric NOE cross peaks in HMQC-NOESY experiments allows for the unambiguous assignment of either cis ([$^{13}C^\alpha$]Xaa,[$^{13}C^\alpha$]Pro) or trans ([$^{13}C^\alpha$]Xaa,[$^{13}C^\delta$]Pro) peptide bonds. The C_i-NOESY-$N_{j+1}H_{j+1}$ experiment is an alternative approach for the identification of H^α-H^α NOEs diagnostic of cis peptide bonds.

Figure 10 illustrates an application of the experiment to a 1.5 mM sample of folded SNase complexed with pdTp and Ca^{2+} (18 kDa). The Lys^{116}–Pro^{117} peptide bond is in the cis configuration in the SNase complex and the H^α protons of the sequential residues Lys^{116} and Pro^{117} are therefore close in space (<2.5 Å). An NOE connecting Lys^{116} H^α to Pro^{117} H^α is indicated in Fig. 10a. Figures 10b and c illustrate the symmetry-related NOEs linking the H^α protons of Ala^{17} and Val^{23}, residing in antiparallel β-strands, β1 and β2, respectively. The H^α chemical shift of Val^{23} (4.65 ppm), which is close to water (at 35 °C), would make such assignments difficult from a conventional experiment recorded on an H_2O sample. Figures 10d and e show symmetry-related NOE peaks between the H^α protons of Met^{26} and Pro^{31}. The near-degeneracy of the H^α chemical shifts of these residues (4.88 and 4.86 ppm, respectively) would render assignment difficult using other 3D NOE experiments.

In principle, it is possible to interchange carbon with proton chemical shift evolution in t_1 so that cross peaks at (ω_{H_i},$\omega_{N_{j+1}}$,$\omega_{HN_{j+1}}$) are detected. However, in the case where the frequencies of H_i and water are degenerate or nearly degenerate, the NOE cross peak of interest may be obscured by exchange/NOE-based cross peaks involving the water resonance. For this reason we favor the version of the experiment which records the carbon chemical shift corresponding to the site of origination of magnetization. Other experiments that have been described above may also be of importance in studies of folded proteins, and their utility is currently under investigation.

Conclusions

A number of triple-resonance pulse schemes for the structural characterization of unfolded, partially folded and folded proteins have been presented, enabling the detection of aliphatic-aliphatic, aliphatic-NH and NH-NH NOEs. The methods have been demonstrated on a ^{15}N,^{13}C-labeled drkN SH3 domain, a partially folded fragment of SNase, Δ131Δ, and a folded SNase complex with pdTp

and Ca^{2+}. In particular, in the case of the drkN SH3 domain and Δ131Δ, the greater resolving power of these new experiments in comparison to conventional NOE experiments has facilitated the recording of unambiguous structural information and the identification of NOEs in both protein systems not detected previously. A more comprehensive study of the patterns of NOEs observed in unfolded proteins is now possible. The combined use of these pulse sequences and conventional ^{13}C- and ^{15}N-edited NOESY experiments should allow a more detailed structural characterization of unfolded or partially folded proteins and enable a greater understanding of the role(s) of preferential structure in the folding and stability of proteins, as well as in biomolecular recognition involving disordered states. Finally, a number of the experiments have significant utility for folded proteins.

Acknowledgements

This work was supported through grants from the Medical Research Council of Canada (J.D.F.-K. and L.E.K.), the National Sciences and Engineering Research Council of Canada (L.E.K.) and the National Institutes of Health, GM34171 (D.S.). The authors thank Dr. Dennis Torchia, NIH, for the gift of folded SNase. O.Z. acknowledges a graduate student fellowship from the Research Institute, Hospital for Sick Children, Toronto.

References

Alexandrescu, A.T., Abeygunawardana, C. and Shortle, D. (1994a) *Biochemistry*, **33**, 1063–1072.

Alexandrescu, A.T., Ng, Y.L. and Dobson, C.M. (1994b) *J. Mol. Biol.*, **235**, 587–599.

Arcus, V.L., Vuilleumier, S., Freund, S.M.V., Bycroft, M. and Fersht, A.R. (1994) *Proc. Natl. Acad. Sci. USA*, **91**, 9412–9416.

Arcus, V.L., Vuilleumier, S., Freund, S.M.V., Bycroft, M. and Fersht, A.R. (1995) *J. Mol. Biol.*, **254**, 305–321.

Bax, A., Clore, G.M. and Gronenborn, A.M. (1990) *J. Magn. Reson.*, **88**, 425–431.

Bax, A. and Pochapsky, S. (1992) *J. Magn. Reson.*, **99**, 638–643.

Bax, A. and Grzesiek, S. (1993) *Acc. Chem. Res.*, **26**, 131–138.

Bax, A. (1994) *Curr. Opin. Struct. Biol.*, **4**, 738–744.

Böhlen, J.-M., Rey, M. and Bodenhausen, G. (1989) *J. Magn. Reson.*, **84**, 191–197.

Boyd, J. and Soffe, N. (1989) *J. Magn. Reson.*, **85**, 406–413.

Buck, M., Schwalbe, H. and Dobson, C.M. (1995) *Biochemistry*, **34**, 13219–13232.

Chazin, W.J., Kördel, J., Drakenberg, T., Thulin, E., Brodin, P., Grundstrom, T. and Forsen, S. (1989) *Proc. Natl. Acad. Sci. USA*, **86**, 2195–2198.

Clore, G.M. and Gronenborn, A.M. (1991) *Annu. Rev. Biophys. Biophys. Chem.*, **20**, 29–63.

Delaglio, F., Grzesiek, S., Vuister, G., Zhu, G., Pfeifer, J. and Bax, A. (1995) *J. Biomol. NMR*, **6**, 277–293.

Dobson, C.M. (1992) *Curr. Opin. Struct. Biol.*, **2**, 6–12.

Ellis, R.J. and Hartl, F.-U. (1996) *FASEB J.*, **10**, 20–26.

Emsley, L. and Bodenhausen, G. (1987) *Chem. Phys. Lett.*, **165**, 469–476.

Farrow, N.A., Zhang, O., Forman-Kay, J.D. and Kay, L.E. (1995) *Biochemistry*, **34**, 868–878.

Fersht, A.R. (1993) *FEBS Lett.*, **325**, 5–16.

Frank, M.K., Clore, G.M. and Gronenborn, A.M. (1995) *Protein Sci.*, **4**, 2605–2615.

Frenkiel, T., Bauer, C., Carr, M.D., Birdsall, B. and Feeney, J. (1990) *J. Magn. Reson.*, **90**, 420–425.

Garrett, D.S., Powers, R., Gronenborn, A.M. and Clore, G.M. (1991) *J. Magn. Reson.*, **95**, 214–220.

Grzesiek, S., Anglister, J. and Bax, A. (1993) *J. Magn. Reson.*, **B101**, 114–119.

Grzesiek, S. and Bax, A. (1993) *J. Am. Chem. Soc.*, **115**, 12593–12594.

Grzesiek, S., Wingfield, P., Stahl, S., Kaufman, J. and Bax, A. (1995) *J. Am. Chem. Soc.*, **117**, 9594–9595.

Harrison, S.C. and Aggarwal, A.K. (1990) *Annu. Rev. Biochem.*, **59**, 933–965.

Hinck, A.P., Eberhardt, E.S. and Markley, J.L. (1993) *Biochemistry*, **32**, 11810–11818.

Ikura, M., Bax, A., Clore, G.M. and Gronenborn, A.M. (1990) *J. Am. Chem. Soc.*, **112**, 9020–9022.

Kadkhodaie, M., Rivas, O., Tan, M., Mohebbi, A. and Shaka, A.J. (1991) *J. Magn. Reson.*, **91**, 437–443.

Kay, L.E., Ikura, M., Tschudin, R. and Bax, A. (1990) *J. Magn. Reson.*, **89**, 496–514.

Kay, L.E., Keifer, P. and Saarinen, T. (1992) *J. Am. Chem. Soc.*, **114**, 10663–10665.

Kay, L.E. (1993) *J. Am. Chem. Soc.*, **115**, 2055–2057.

Kay, L.E., Xu, G.Y. and Yamazaki, T. (1994) *J. Magn. Reson.*, **A109**, 129–133.

Kay, L.E. (1995) *Prog. Biophys. Mol. Biol.*, **63**, 277–299.

Kupce, E. and Freeman, R. (1995) *J. Magn. Reson.*, **A115**, 273–276.

Kupce, E. and Wagner, G. (1995) *J. Magn. Reson.*, **B109**, 329–333.

Logan, T.M., Olejniczak, E.T., Xu, R.X. and Fesik, S.W. (1993) *J. Biomol. NMR*, **3**, 225–231.

Logan, T.M., Theriault, Y. and Fesik, S.W. (1994) *J. Mol. Biol.*, **236**, 637–648.

Loll, P.J. and Lattman, E.E. (1989) *Proteins Struct. Funct. Genet.*, **5**, 183–201.

Marion, D., Ikura, M., Tschudin, R. and Bax, A. (1989) *J. Magn. Reson.*, **85**, 393–399.

Mayer, B.J., Hamaguchi, M. and Hanafusa, H. (1988) *Nature*, **332**, 272–275.

McCoy, M. and Mueller, L. (1992) *J. Am. Chem. Soc.*, **114**, 2108–2110.

McCoy, M. (1995) *J. Magn. Reson.*, **B107**, 270–273.

Montelione, G.T., Lyons, B.A., Emerson, S.D. and Tashiro, M. (1992) *J. Am. Chem. Soc.*, **114**, 10974–10975.

Morris, G.A. and Freeman, R. (1979) *J. Am. Chem. Soc.*, **101**, 760–762.

Muhandiram, R. and Kay, L.E. (1994) *J. Magn. Reson.*, **103**, 203–216.

Neri, D., Billeter, M., Wider, G. and Wüthrich, K. (1992) *Science*, **257**, 1559–1563.

Olivier, J.P., Raabe, T., Henkemeyer, M., Dickerson, B., Mbamalu, G., Margolis, B., Schlessinger, J., Hafen, E. and Pawson, T. (1993) *Cell*, **73**, 179–191.

Pascal, S.M., Muhandiram, D.R., Yamazaki, T., Forman-Kay, J.D. and Kay, L.E. (1993) *J. Magn. Reson.*, **B103**, 197–201.

Patt, S.L. (1992) *J. Magn. Reson.*, **96**, 94–102.

Pawson, T. (1995) *Nature*, **373**, 573–580.

Rassow, J. and Pfanner, N. (1996) *Curr. Biol.*, **6**, 115–118.

Schleucher, J., Sattler, M. and Griesinger, C. (1993) *Angew. Chem. Int. Ed. Engl.*, **32**, 1489–1491.
Shaka, A.J., Keeler, J., Frenkiel, T. and Freeman, R. (1983) *J. Magn. Reson.*, **52**, 335–338.
Shaka, A.J., Lee, C.J. and Pines, A. (1988) *J. Magn. Reson.*, **77**, 274–293.
Shortle, D. (1993) *Curr. Opin. Struct. Biol.*, **3**, 66–74.
Shortle, D. (1996) *Curr. Opin. Struct. Biol.*, **6**, 24–30.
Simon, M.A., Dodson, G.S. and Rubin, G.M. (1993) *Cell*, **73**, 169–177.
Spolar, R.S. and Record Jr., M.T. (1994) *Science*, **263**, 777–784.
Stonehouse, J., Shaw, G.L., Keeler, J. and Laue, E.D. (1994) *J. Magn. Reson.*, **B107**, 178–184.
Torchia, D.A. (1984) *Annu. Rev. Biophys. Bioeng.*, **13**, 125–144.
Torchia, D.A., Sparks, S.W. and Bax, A. (1989) *Biochemistry*, **28**, 5509–5524.
Van Halbeek, H. (1994) *Curr. Opin. Struct. Biol.*, **4**, 697–709.
Venters, R.A., Metzler, W.J., Spicer, L.D., Mueller, L. and Farmer II, B.T. (1995) *J. Am. Chem. Soc.*, **117**, 9592–9593.
Vuister, G.W. and Bax, A. (1992) *J. Magn. Reson.*, **98**, 428–435.
Wüthrich, K. (1986) *NMR of Proteins and Nucleic Acids*, Wiley, New York, NY, U.S.A.
Wüthrich, K. (1994) *Curr. Opin. Struct. Biol.*, **4**, 93–99.
Zhang, O., Kay, L.E., Olivier, J.P. and Forman-Kay, J.D. (1994) *J. Biomol. NMR*, **4**, 845–858.
Zhang, O. and Forman-Kay, J.D. (1995) *Biochemistry*, **34**, 6784–6794.
Zhu, G. and Bax, A. (1990) *J. Magn. Reson.*, **90**, 405–410.
Zhu, G. and Bax, A. (1992) *J. Magn. Reson.*, **98**, 192–199.